Graduation thesis,

Faculty of Science,

2022.

Quantitative measurement and simulation of perceptual intensity in the vanishing illusion.

Field NameMaterials Science

Student registration no.

192052 Mr.　Name

Taiyo Kono

Supervisory teacher Michelette　Rudzero.

Submitted on 1 January 2023.

Submitted on 1 January 2023

Table of Contents

1 Chapter　Introduction Theory

1.1　background

Illusion research has been conducted for a long time, but with the recent development of perceptual psychology and neuroscience, it has become a field that attracts even more attention. In particular, since the beginning of the 2000s, visual illusions have been increasingly featured in TV programmes, commercials and magazines, and we feel that visual illusions have become more familiar to us. Thanks to the activities of the mass media, many people are now aware of the existence of optical illusions. On the other hand, most of us do not understand the structure and mechanism of visual illusions, the mechanism of the generation of illusions, and the benefits of research on visual illusions for our daily lives. Traditionally, the generation of illusions has been regarded as a bug in the brain. However, recent illusion research has quantified illusions, and some of the mechanisms that generate illusions are now better understood. In the course of research, it has been reported that the illusory effects of existing illusions can be strengthened or weakened by generating new illusions by computer or by extracting the part of the illusory effect that is caused by the illusory effect.
(Arai and Arai, 2012)

Furthermore, people obtain most of their stimuli from the outside world through vision. In other words, a full understanding of the mechanisms of visual illusions caused by human vision is very important for understanding the human brain. Thus, illusion research is closely related to human brain research, and advances in illusion research can advance brain research. At present, a mathematical model of the human brain has not yet been completed and only partial models of the brain exist. Therefore, it is expected that illusion research can be used as one clue to the completion of a whole-brain model of the brain. Thus, illusion research is also meaningful from the perspective of studying the brain. It has also been reported that the findings obtained from illusion research can be effectively utilised in our daily life, in addition to brain research. In fact, the findings obtained from illusion research can be applied to medical care, welfare, architecture, transportation, environmental design and other engineering fields related to the mechanisms of the cranial nervous system, thereby helping to solve problems in the real world.

1.2 research objectives

The aim of this study is to elucidate the mechanism of new illusory figures whose generation mechanism has not yet been elucidated. For this purpose, quantitative measurement of the illusion effect, its analysis and simulation of the firing of neurons during the observation of illusion images are conducted. To quantitatively measure the illusion effect, we conduct perceptual experiments with subjects, collect and analyse the data. There are no previous studies that have quantitatively measured and analysed this illusion image, and it can be said to be novel. In the simulation, the ON-centred receptive field model is used to simulate the firing of neurons in the retinal receptive field when the illusion is observed. The aim of this simulation is to qualitatively observe the effect of the illusion. As mentioned above, the illusion

The findings from visual research can be applied to brain research and various other fields to help solve real-world problems. The ultimate goal of this research is also to understand brain algorithms through visual illusions.

2 Chapter-related research research

2.1 Definition of optical illusions

In the present study, a perceptual experiment was conducted using illusion figures. Therefore, we first check the definition of the phenomenon called illusion. When considering the definition of an illusion, it is good to consider several illusions. For example, one of the most famous illusions is the Müller-Lyer illusion (Nicola Bruno, *et al.* 2009) (Figure 2-1A). In this illusion, one segment appears to be longer than the other due to the different orientations of the arrow feathers drawn above and below, even though the lengths of the two segments are the same. There is another illusion called the Necker cube (Fig. 2-1B). When a projection of a cube is drawn on a plane, the two-dimensional projection appears as if it were there in three dimensions. Furthermore, it is known that this illusion can be seen in two different ways, depending on how you look at it (J. mason, et al. (J. mason,*et al.* 1973)

Thus, an optical illusion states that when some figure is given as an input to a certain visual information processing system, such as the brain, a perception deviating from the prediction from that system is produced. This is called an illusion, and the figure that produces it is called an illusory figure. (Murakami, 2010) A rough classification of illusion figures has been submitted by Gregory et al. (Gregory, *et al.* 1998). (Gregory, et al. 1998) However, it has been reported that illusions are merely the final output results of multi-stage information processing in the brain and cannot be clearly classified. (Murakami, 2010)

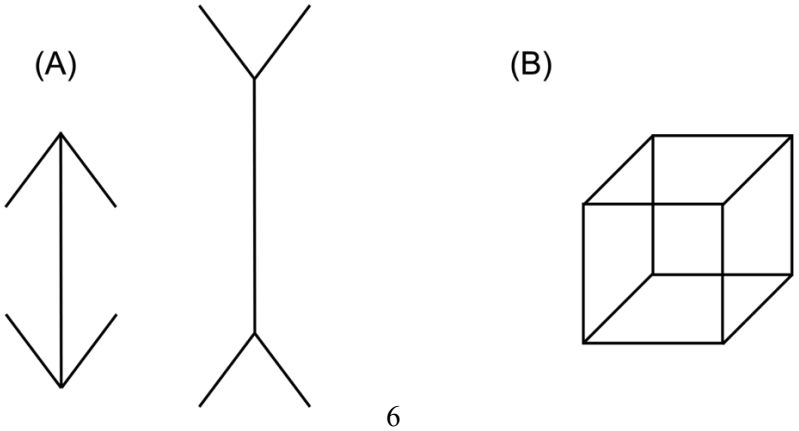

Figure 2-1 (A) Müller-Lyer illusion. In reality, the lengths of the left and right central line segments are equal, but they appear to be different when the directions of the arrow feathers in the upper and lower parts are opposite. (b) Necker cube. The figure is a two-dimensional projection of a cube, but it appears to be three-dimensional. It can be seen in two ways depending on which side is regarded as the front.

2.2 Illusion as a research tool

Section 2.1 provided a definition of illusions. In this section, we discuss why illusions are used in brain research.

In general, most of us humans perceive the relationship between stimuli from the outside world and our brain's perception as if it were a constant map. In fact, if you saw a red strawberry in a supermarket, you would not doubt that it was a red strawberry. However, our perceptions, including this one, are merely the output of our brain as perceptions based on all the stimuli from the real world. Therefore, red strawberries are in fact "strawberries that look red". When we see red strawberries, it does not mean that red strawberries exist in the real world. The colour of strawberries is based on visible light reflected from the surface of the strawberry and detected by the retina, which is then used by the brain to create a "red" strawberry in the brain. There is also an optical illusion that utilises the brain's colour perception, which is called colour constancy. Colour constancy is the effect that the surface colour perceived by the brain remains constant, regardless of the spectral changes in the surrounding illumination (G. Monge, 1789) Figure 2-2 below shows an illusion using colour constancy created by Akiyoshi Kitaoka of Ritsumeikan University. Note that Kitaoka states that the strawberries depicted in the illusory image appear to be red, but this is not caused by our knowing that strawberries appear to be red (Figure 2-2).

Thus, it is important to remember that the external world that we take for granted is in fact a fiction created by the brain. Normally, when investigating visual information processing in the human brain, it would be impossible from an ethical point of view to directly measure and manipulate the inner workings of the visual system. If we define illusion as described in section 2.1, it can be interpreted as a discrepancy between the input and output of the brain. By investigating this discrepancy between input and output (i.e. external stimuli and brain perception), it is possible to estimate the behaviour of the brain's information processing mechanisms and algorithms. Even if we exclude ethical considerations, the input-output relationship we usually perceive, such as a constant mapping, does not provide clues to the mechanism when investigating the mechanisms of the visual system. This is also where optical illusions are useful. Input
-Studies of brain algorithms are carried out by using optical illusions that produce a displacement between outputs, and by quantitatively measuring and analysing the displacement that occurs.

Figure 2-2 Illusion based on colour constancy. The strawberry in the left image above does not have red pixels due to the light blue filter, but appears to be red due to brain compensation. In addition, the strawberry in the right image appears to be blue, though it has no blue pixels due to the yellow filter.

(Cited from: https://www.ritsumei.ac.jp/research/radiant/heart/story10.html/ Last accessed.
24/01/2023)

2.3 About the viewing angle

When observing the illusion images used in this study, it is important to know which size of the illusion image is being observed. The visual angle is explained in this section. The visual angle is the angle formed when an observed object is projected onto the retina (Fig. 2-3) If the visual angle is equal, the size of the image projected onto the retina is
The brain perceives the same size because the sizes are equal. In addition, each degree of visual angle is referred to as a unit visual angle and
Called. The viewing angle is determined by the following equation.

$$V = \frac{360}{\pi} \quad arctan \frac{s}{2d0} \quad 1\,\text{unit}: °2$$

Using the above equation, the viewing angle during the observation of the optical illusion in this research experiment was calculated (Table 2-1) The observation distances D were 50 cm and 100 cm, and the size of the observed object

(illusory image) was 8.0 cm, which is the size on the actual PC display.

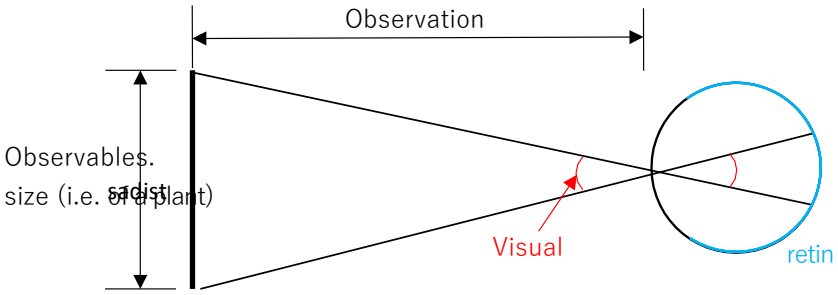

Figure 2-3. Schematic diagram of the viewing angle.

Table 2-1. Size of the visual angle in each experiment.

	Experiment 1-1.	Experiments 1-2 2-1	Experiment	Experiment 2-2.
Visual angle (°)	9.147	4.581	9.147	9.147

2.4 Spatial frequency characteristics of vision and contrast sensitivity functions.

The illusion used in this study (Fig. 3-5) is a mask image with a high-frequency component of light-dark contrast. Spatial frequency is defined as the number of cycles of light and dark sinusoids within a unit viewing angle (2.3), and its unit is cycle/degree = cpd (cycles per degree). In general, the spatial frequency response has either a band-pass characteristic, which passes both high and low frequencies, or a low-pass characteristic, which passes low frequencies, with maximum sensitivity around 10 cpd (J.G. Robson, 1966) Under low luminance, the sensitivity in the low spatial frequency band is also depressed.

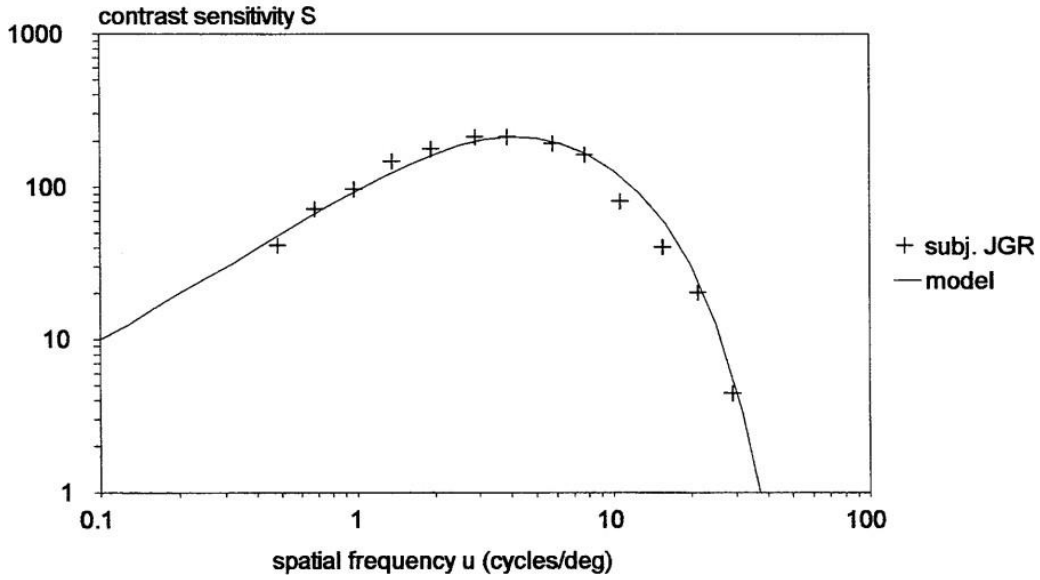

Figure 2-4 Contrast sensitivity function. Contrast sensitivity is plotted on an arbitrary logarithmic scale against spatial frequency. (Cited by J.G. Robson, 1966)

2.5 hybrid image

In relation to the spatial frequency properties of vision described in section 2.4, in 2006 Oliva, Torralba and Schyns

Hybrid images with two different views depending on the viewing distance were proposed by

(Oliva.A *et al.* 2006) It was created by compositing two images, one with a high spatial frequency and the other with a low spatial frequency. The hybrid image is an optical illusion that makes use of the fact that when people perceive an image, they adopt a spatial frequency band that depends on the size of the viewing angle. Specifically, when perceiving this image at close range, i.e. when the viewing angle is small, only the high-frequency component image is seen. On the other hand, at a distance, i.e. when the viewing angle is large, only the low-frequency component image is seen and an effect occurs. Furthermore, in 2012, Arai et al. at Waseda University reported a super-hybrid image in which three types of visibility exist depending on the distance (Arai and Arai, 2012)

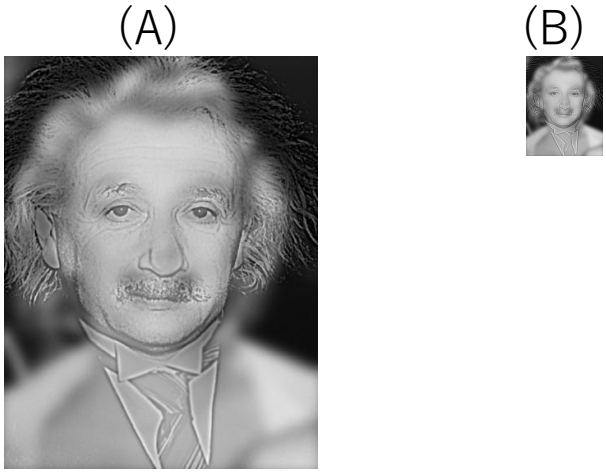

Figure 2-5. Hybrid image by Oliva, A. Einstein when observed at close range. Marilyn Monroe is visible when observed at a distance.

(cited at: http://olivalab.mit.edu/hybrid_gallery/gallery.html) (Last accessed 24/01/2023)

3 Chapter Experimental overview Summary

3.1 About PsychoPy

There are several reasons for using Python to create perceptual experiments, but the main reason is that Python has a number of packages oriented towards perceptual and psychological experiments. A package is something that extends the functionality of Python by incorporating it into Python, and by combining various packages, you can create experiments that suit your needs.

PsychoPy is one of the packages of the Python library, and is a tool that allows psychological experiments to be easily created on a personal computer (PC). The introduction of PsychoPy into experiments makes it possible to automatically control operations that are too complicated to be carried out manually, such as recording the reaction time of each subject and accumulating the resultant data, in perceptual experiments, using a PC. In addition, PsychoPy can be used to create experiments with relative ease, even when multiple conditional branches and dynamic processing are involved, as in this experiment.

There are two main ways to create experiments in PsychoPy. The first is Psychopy Coder, where you write the Python code yourself to create the experiment, and the second is Psychopy Builder, where you can easily create experiments by arranging icons on the GUI app. Psychopy Coder requires the creator of the experiment to write the Python code themselves, which requires some familiarity with Python programming. Psychopy Builder, on the other hand, allows users to construct and create experiments by simply rearranging icons on the GUI application, so even those who have never written a Python programme can create experiments more easily than with PsychoPy Coder. However, if the experiments to be created are complex, it is difficult to handle the creation of experiments using only Psychopy Builder. Thus, by introducing PsychoPy and using PsychoPy Coder and PsychoPy Builder separately or in combination as necessary, it is possible to create experiments appropriately.

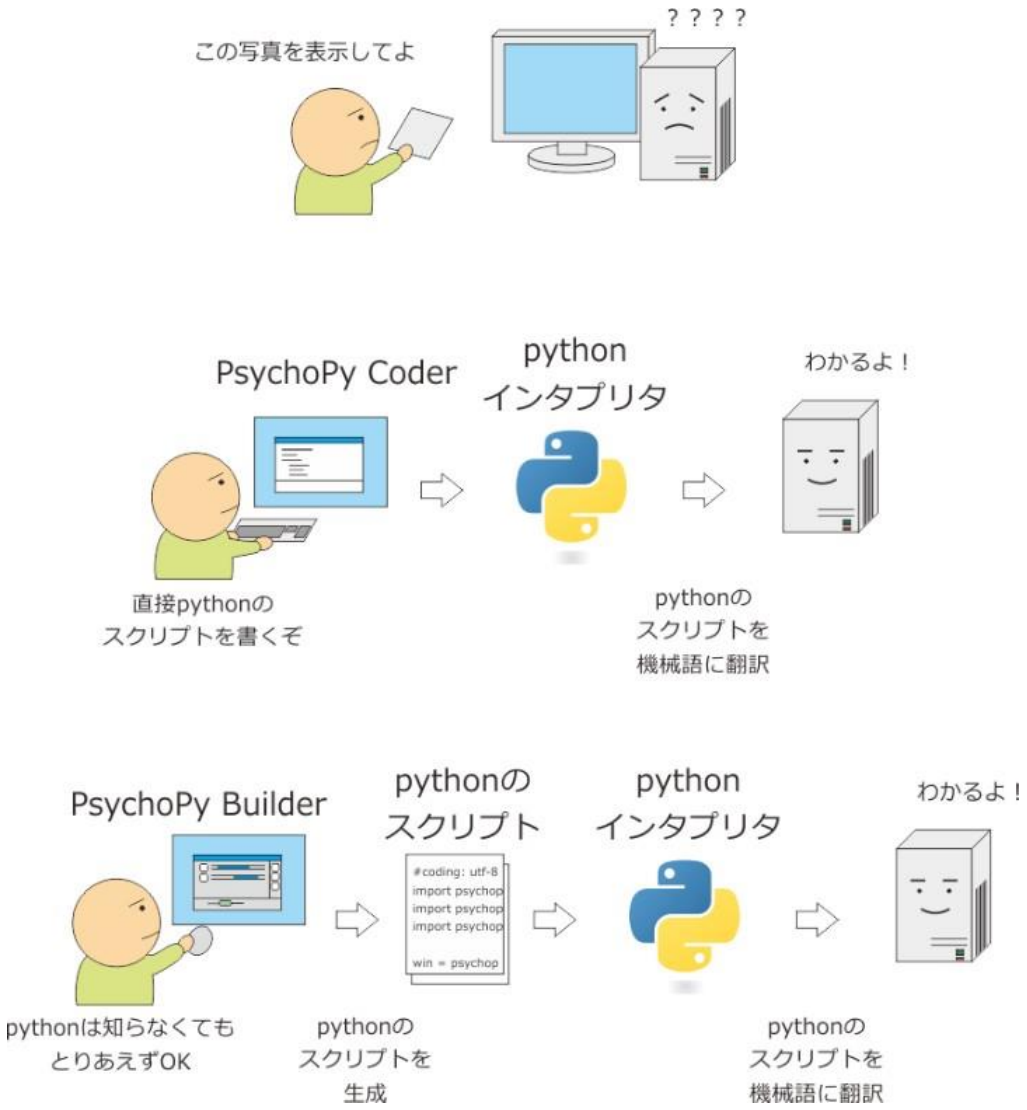

Figure3-1 Operational images of PsychoPyCoder and PsychoPy Builder. As shown above, PsychoPy Coder requires the experiment creator to write the Python scripts themselves. In PsychoPy Buil der, on the other hand, PsychoPy creates the Python scripts for you, making it easier to create experiments.

(cited at: http://www.s12600.net/psy/python/ppb/PsychoPyBuilderBook.pdf) (Last accessed 24/01/2023)

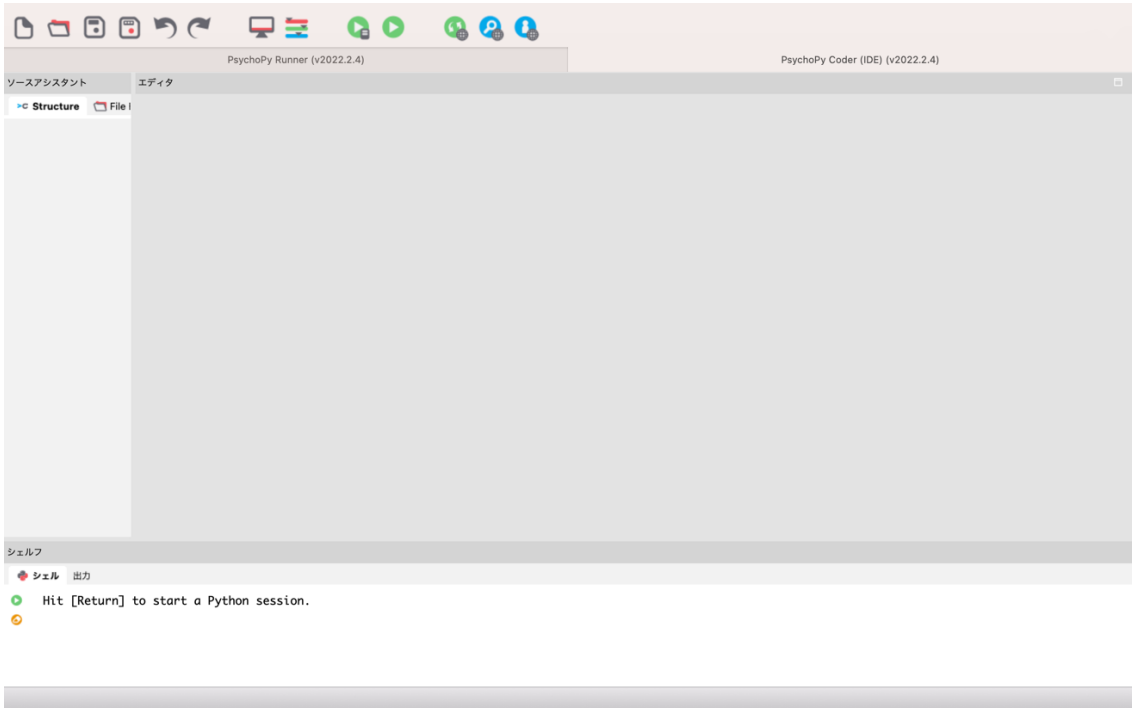

Figure 3-2 Initial screen of PsychoPy Coder, where experiments are created from scratch by writing Python code directly.

Figure 3-3 PsychoPy Builder experiment creation screen. It consists of three panes, where the stimuli etc. selected in the component pane are placed in the routine pane, and the order of the routines is determined in the flow pane.

Figure3-4 PsychoPyRunner experiment add screen. When an experiment is selected and the Run button on the right is clicked, a window for entering the subject name and session appears and the experiment starts.

3.2 Experimental environment and subjects

The subjects were 18 male and 18 female adults, all of whom had clear eyes (including those with corrective glasses, contact lenses, etc.). Before the start of the experiment, the subjects were given instructions on how to operate the PC and the structure of the experiment in the experiment manual (see p.) displayed on the display, so that each subject could operate the experiment appropriately. To ensure fairness in the results, subjects were not informed of the purpose of the experiment. The experiment was conducted over a two-week period from 1 to 15 December 2022, all in a room in the Science Research Building at Yokohama City University. Furthermore, to ensure that the subjects could concentrate on the experiment in a quiet state, they were not spoken to more than necessary.

3.3 Experimental equipment and vanishing illusions

The display size of the PC (MacBook Retina, 12-inch, 2017) used in this study was 12 in. The Cambodia is 28.05 cm wide and 19.65 cm high, with a width of 28.05 cm and a height of 19.65 cm (2304 x 1440).

Figure 3-5 shows the illusion image used in this study. This illusion, the existence of which was suggested by Akiyoshi Kitaoka of Ritsumeikan University, is that when a mask image with high spatial frequency components is superimposed on a background image of letters or illustrations, the background image is hidden by the mask image and is difficult to be seen. Quantitative measurement of the illusory effect of this illusion has not yet been conducted, and the mechanism of the generation of the illusory effect of this illusion has not been clarified. In the experiment, a square with one side of 8.0 cm was displayed on the right side of a PC display. The spatial frequency of this illusory figure varied from experiment to experiment. In Experiments 1-1.2-1 and 2-2, the distance between the subject and the display was 50 cm, so the viewing angle was obtained as shown in Table 2-1 and the spatial frequency was 8.7460 cpd. On the other hand, in Experiments 1-2, the distance between the subject and the display was set to 100 cm, so the spatial frequency was 17.492 cpd based on the same calculation.

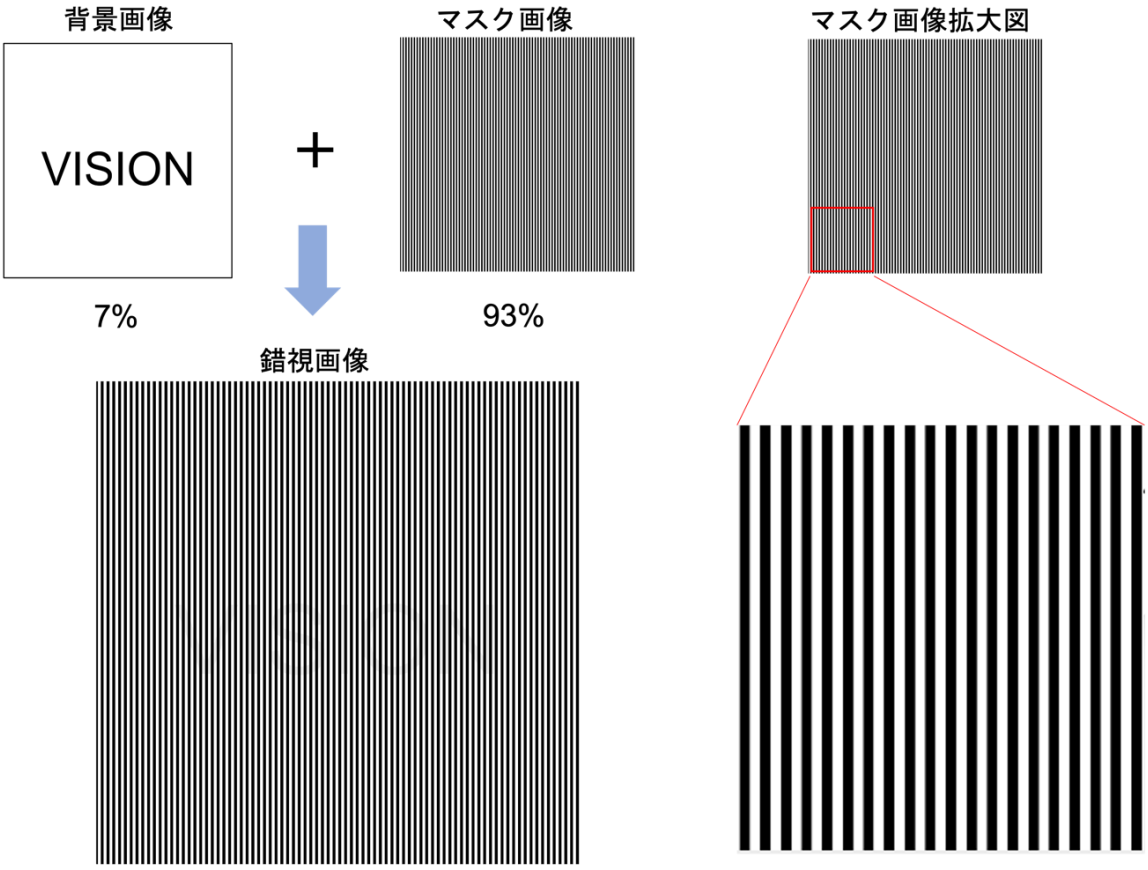

Figure 3-5 Structure of the vanishing illusion image used in this study. As shown above, the illusion effect is created by superimposing a background image with text strings or illustrations and a mask image with high spatial frequency components, adjusting the transparency.

3.4 experimental configuration

Subjects were subjected to four types of experiments. These experiments can be classified into two types: static and dynamic illusions. In the experiment with the static illusion, (1-1) the distance between the subject and the PC display was fixed at 50 cm. (1-2) The distance between the subject and the PC display is fixed at 100 cm. We measured how the illusory effect of the illusory image on the subject changed with each observation distance. In the experiment using the stationary illusion, mask images with five different spatial frequency characteristics (Fig. 3-6) were used, so that the illusory effects between the mask images were compared at the same time. In the experiment using the dynamic illusion, (2-1) only the mask image is made to drift at a specific temporal frequency. (2-2) The entire illusory image is subjected to a single oscillation in two directions, horizontally and vertically, at a specific time frequency. The effect of the illusion was measured. Changes in the illusory effect caused by the above two operations were measured.

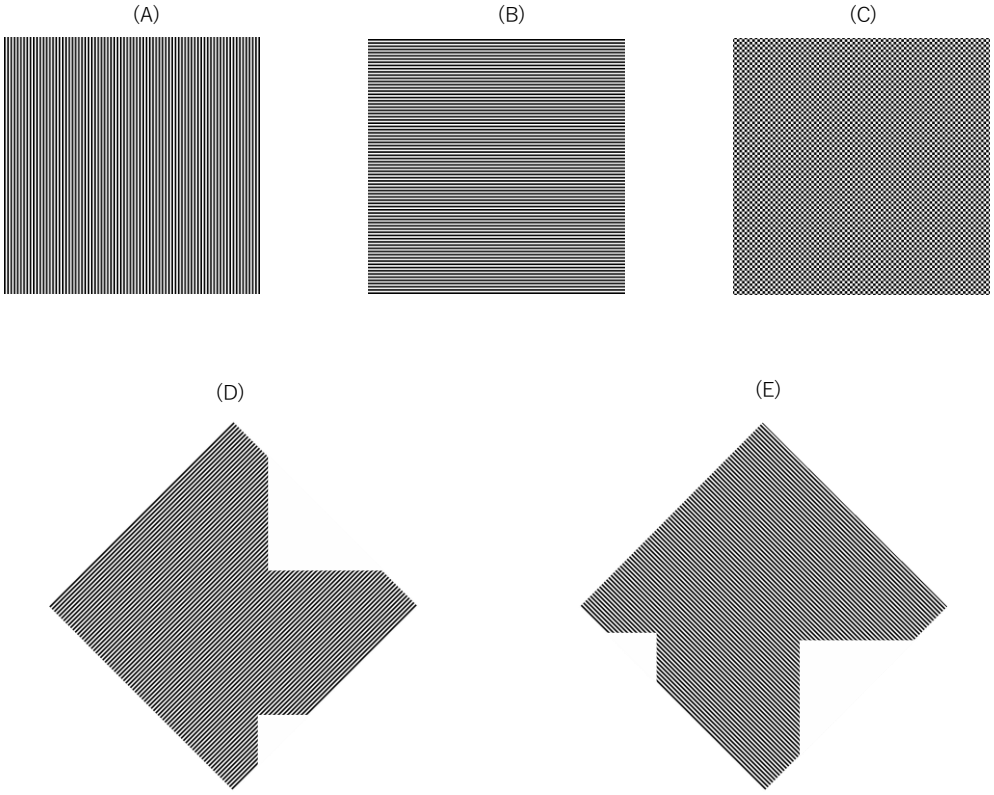

Figure 3-6 Five mask images used in experiment (1).(A) vertical stripe, (B) horizontal stripe, (C) checkerboard (D), right oblique stripe, (E) left oblique stripe. (The spatial frequency of the (A),(B),(D) and (E) stripes was 80 Hz, the spatial frequency of the

(C) checkerboard pattern was set at 50 Hz intervals between the vertical and horizontal stripes.

3.5 experimental procedure

The experiment was conducted on PsychoPy on a PC according to the experimental operation manual (Figure 3-7) shown to the subjects. First, subjects were asked to sit on a chair facing the experimental PC display on their desk. The subjects were then familiarised with the experimental manipulations by means of the manual before starting the experiment. The operation itself was simple, as the subjects only had to click on three buttons on the screen during the experiment. Subjects adjusted the transparency so that the target text image (left of the experimental screen), which was displayed with random densities, and the text image in the illusion image (right of the experimental screen) were perceived as equally dense. This manipulation was repeated in Experiment 1-1 described in section 3.4
to 2-2 were carried out in sequence.

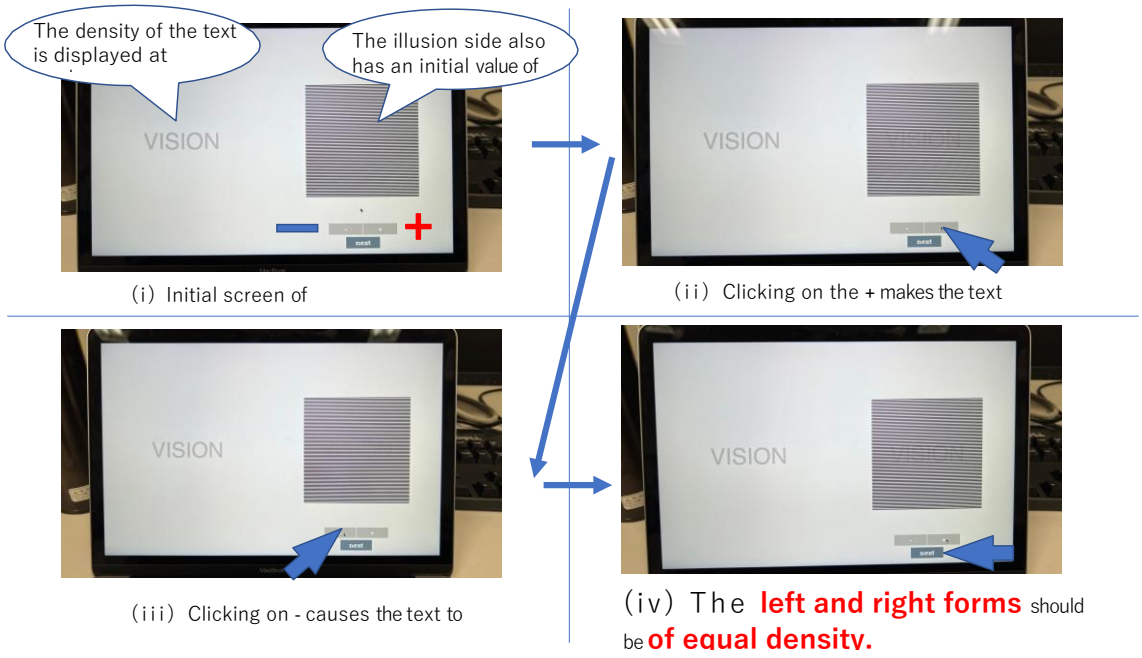

Figure 3-7 Operation manual shown to subjects at the start of the experiment. The actual experimental screen was also shown on a similar PC display.

4 Chapter 3: Results and analysis of visual illusion effects.

4.1 Verification of illusion effects with static illusions.

4.1.1 In Sections 4.1.1 and 4.1.2, the illusory effects of stationary illusory images were measured; in Section 4.1.1, the results of the comparison of illusory effects for each of the five types of mask images are presented, and in Section 4.1.2, the experimental results of the illusory effects at changes in observation distance are presented.

4.1.1 Comparison of the illusion effect of each masked image

The experimental results for each of the five mask images are shown below. Figure 4-1 shows the results at an observation distance of 50 cm. In each illusion image, the mask images were (A) vertical stripes, (B) horizontal stripes, (C) checkerboard (D) right oblique stripes and (E) left oblique stripes. The horizontal axis of each scatter plot took the actual intensity of the letters displayed on the left side of the experimental screen, while the vertical axis took the intensity perceived by the subject. The red dashed line in the diagram represents the straight line with slope 1. In other words, the point on the red dashed line is the point where the intensity of the target text image actually displayed equals the intensity of the text in the illusion image perceived by the subject. The area above the dashed line is the area where the subject has difficulty perceiving the text in the background due to the illusory effect of the mask image. On the other hand, the lower area of the line is the area where the text appears darker rather than the actual text intensity. Figure 4-1, (a) in Figure 4-2~.

(In (e), in the part of the image where the abscissa value is less than 0.1, many of the points are located in the region above the dashed line. This indicates that the illusion effect occurs in this region. Conversely, when the intensity of the displayed text exceeds 0.1, the illusion effect is reduced and the points are plotted in the region below the dashed line. The tests of normality and equal variance between each mask image yielded $p>0.05$, respectively, and the null hypothesis was adopted. The results of one-

dimensional ANOVA without correspondence showed $p<0.05$, indicating that differences in mask images may have an influence on the illusion effect. Following the one-dimensional ANOVA, multiple comparisons were conducted using Tukey's test to investigate which mask images had significant differences. As a result, significant differences in the illusion effect were found in the chequered pattern - horizontal stripes, chequered pattern - right oblique stripes and chequered pattern - left oblique stripes (Table 4-1).

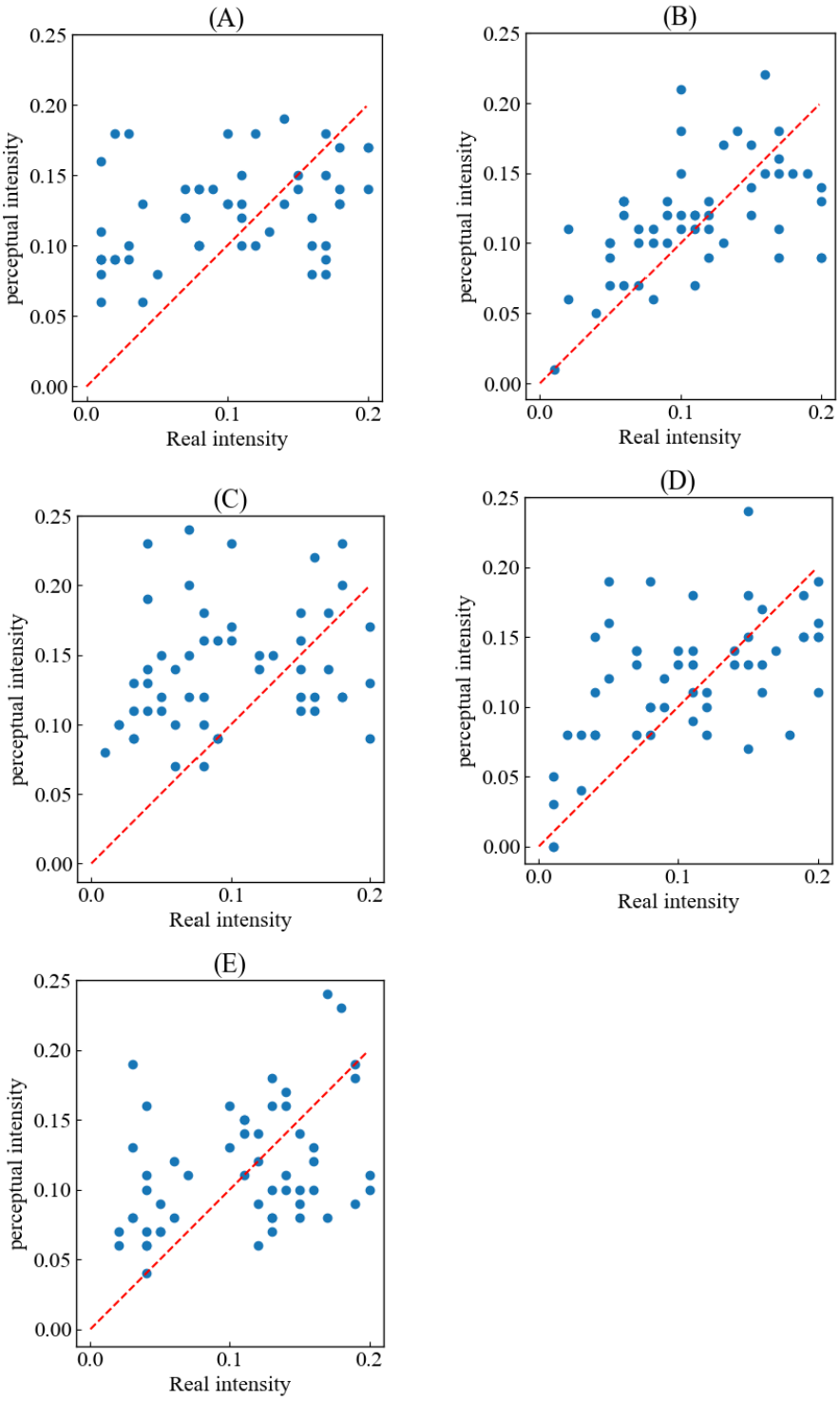

Figure 4-1 Comparison for each of the five mask images. (A) vertical stripes, (B) horizontal stripes, (C) checkerboard (D), right oblique stripes, (E) left oblique stripes. The horizontal axis represents the intensity of the actual displayed letter, while the vertical axis represents the subject's perceived intensity of the letter. The red dashed line in the diagram

represents the straight line with slope 1.

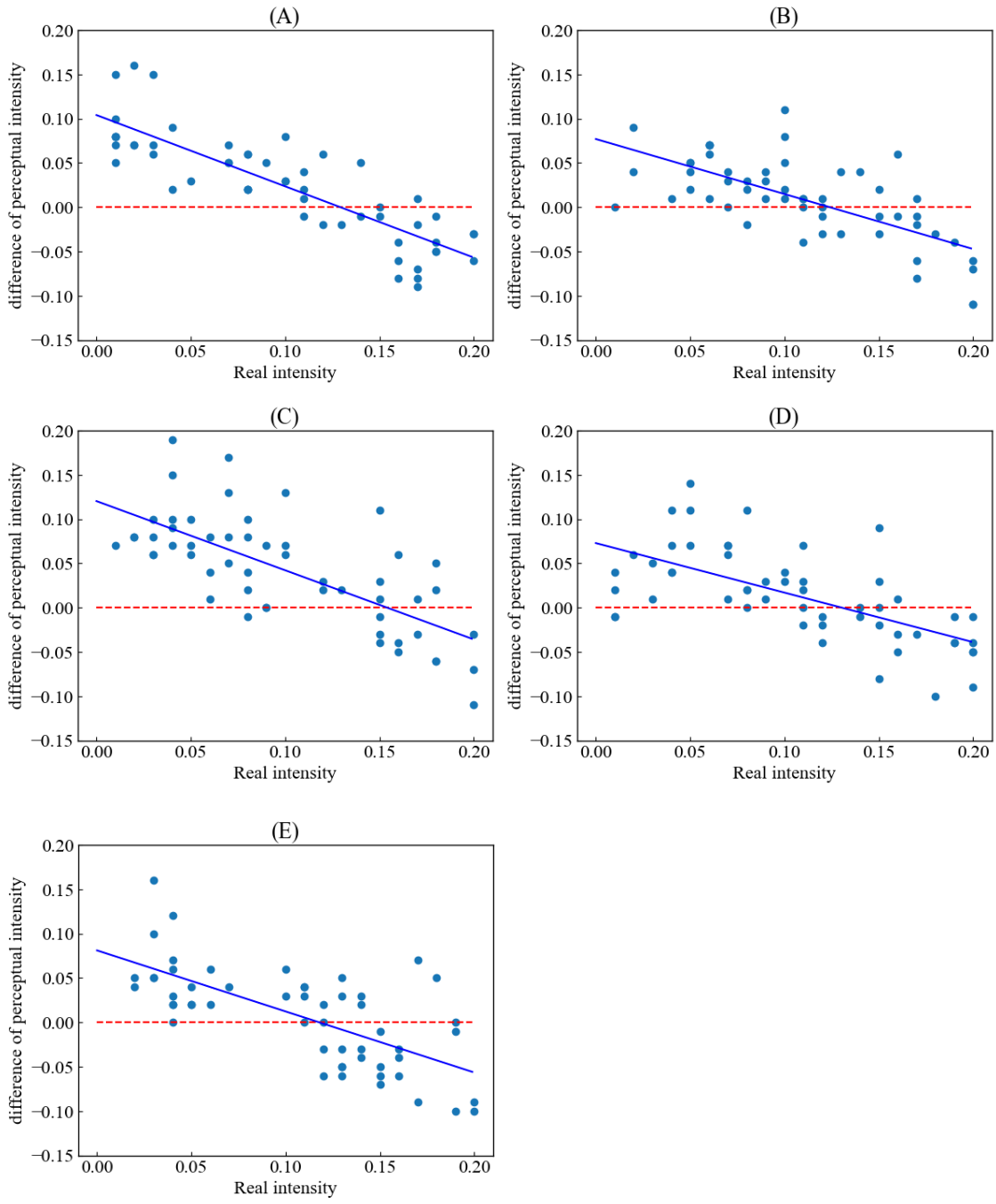

Figure 4-2 Graph with the vertical axis of Figure 4-1 changed to the difference from the horizontal axis. The red dashed line in the figure is the actual text

This is the line where the difference between the intensity of the letters perceived by the subject and the intensity of the letters is 0. In other words, the illusion effect occurs at points in the upper region of this line. The blue line in the figure is the approximate straight line of the

measured values.

Table 4-1. Results of Tukey's multiple comparison test between each masked image. Significance level 0.05

Mask image 1	Mask image 2	p-value
vertical stripes	horizontal stripes	0.6387
vertical stripes	checkerboard	0.3865
vertical stripes	right oblique stripe	0.8691
vertical stripes	oblique left stripe	0.5266
horizontal stripes	checkerboard	0.0148
horizontal stripes	right oblique stripe	0.9937
horizontal stripes	oblique left stripe	0.9998
checkerboard	right oblique stripe	0.0495
checkerboard	oblique left stripe	0.0085
right oblique stripe	oblique left stripe	0.9768

4.1.2 Relationship between observation distance and illusion effect.

The results when the illusory images were observed from a distance of 50 cm and at a distance of 100 cm were superimposed on the graphs. For each of the mask images (A)~(E), the subject's perceived intensity decreased at an observation distance of 100 cm more than at an observation distance of 50 cm (Fig. 4-3). Furthermore, the linear approximation for 50 cm and 100 cm respectively is evident from the overall shift of the straight line downwards (Fig. 4-4). Based on Figure 4-4, a histogram was created. Based on this histogram, a t-test was performed between the observation distances of 50 cm and 100 cm. As a result, significant differences were found between the observation distances of 50 cm and 100 cm for all mask images (Table 4-2).

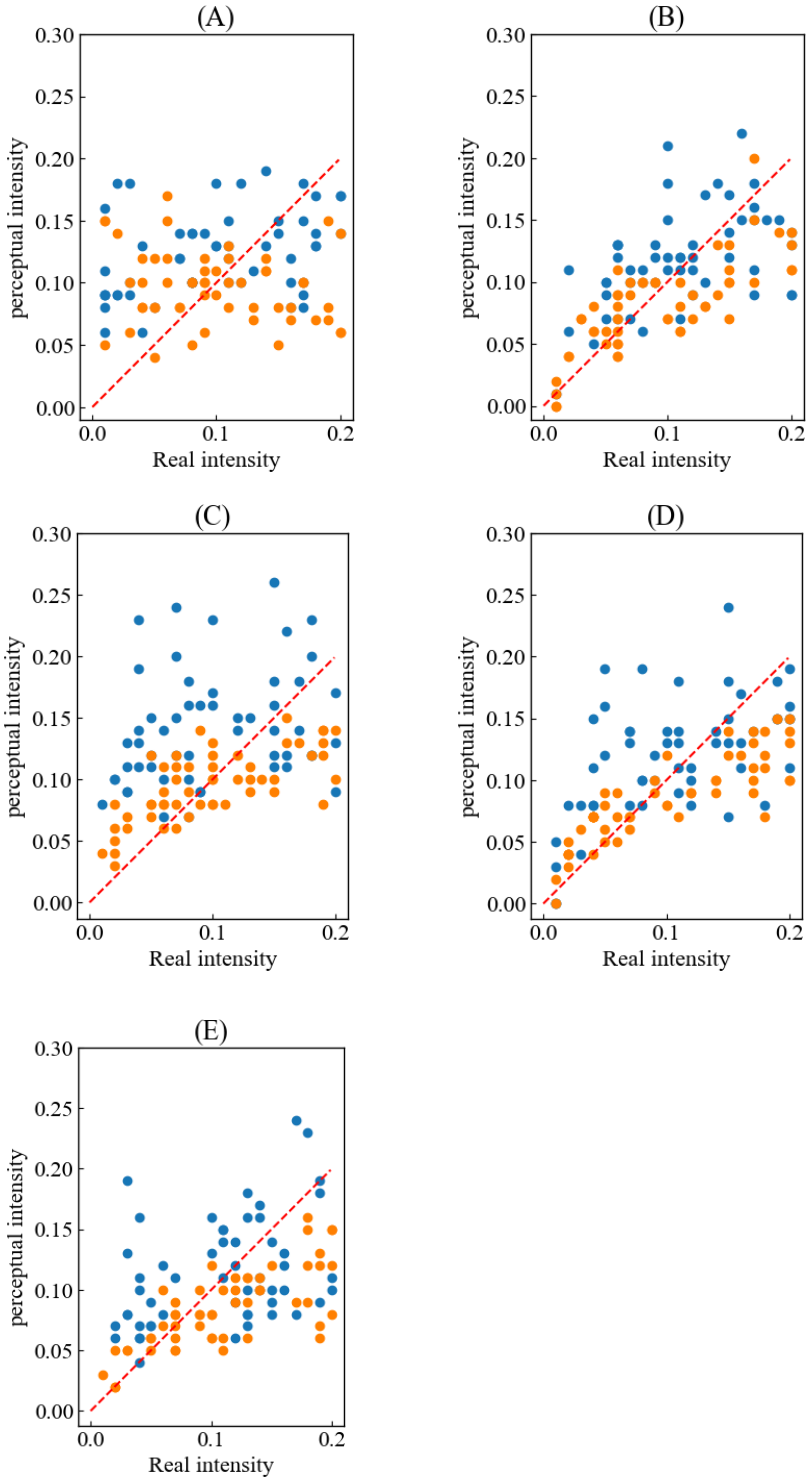

Figure 4-3 Comparison of results at an observation distance of 50 cm (blue) and 100 cm (orange).(A) vertical stripes,(B) horizontal stripes,(C) chequered pattern,(D) right oblique stripes,(E) left oblique stripes. For all mask images, the perceived intensity is reduced at an observation distance of 100 cm compared to an observation distance of 50 cm.

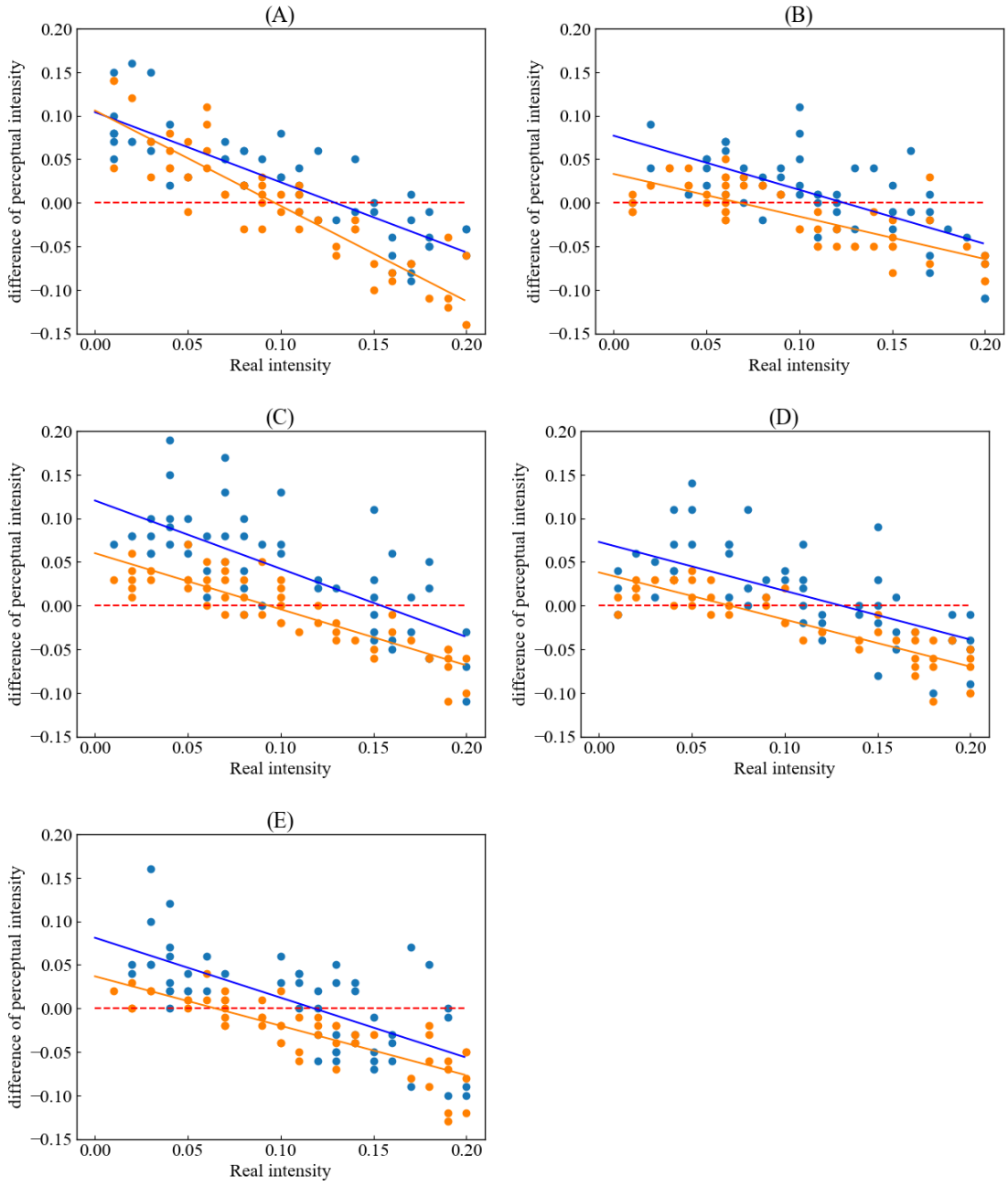

Figure 4-4 Graph with the vertical axis of Figure 4-3 changed to the difference from the horizontal axis. In each of the approximate lines, the solid orange line of the 100 cm approximate line is also shifted downwards more generally than the solid blue line of the 50 cm approximate line.

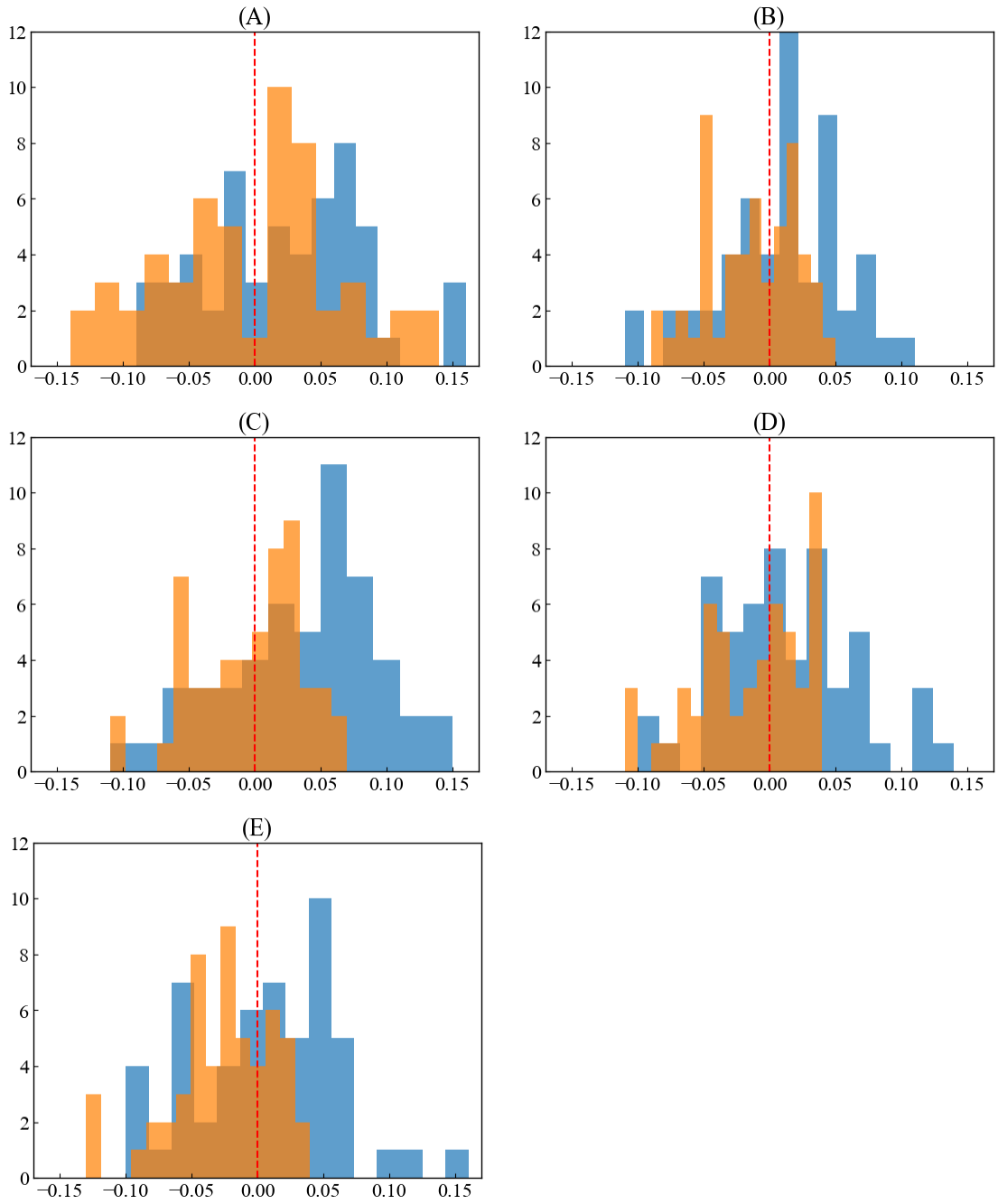

Figure 4-5. Histogram created from Figure 4-4.(A)~(E) for each masked image at an observation distance of 50

The observation distance of 100 cm (orange) is shifted to the left compared to 100 cm (blue).

Table 4-2 Results of t-tests for 50 cm and 100 cm observation distances.

Significance level 0.05

Type of mask image	p-value
Vertical stripes	0.031
horizontal stripes	0.008
chequered pattern	1.70e-05
Right diagonal stripe	0.001
Left diagonal stripe	5.00e-04

4.2 Verification of illusion effects by dynamic illusions.

4.2 Section 4.2.1 shows the results when the mask image (vertical and horizontal stripes) in the illusion image is made to drift at a specific frequency, and Section 4.2.2 shows the results when the whole illusion image is made to oscillate in two directions (horizontal and vertical). The results are shown in Section 4.2.2.

4.2.1 Illusionary effects associated with drift in mask images.

Experimental results are shown below when two types of mask images, vertical and horizontal stripes, were drifted at a specific time frequency. The temporal change of the mask image was changed by drifting the phase of the mask image; PsychoPy has a function that allows n Hz drift by setting n*t to the phase of the stimulus. Here n Hz is the number of cycles per unit time. In the present study, the time frequencies of the drift in the mask image were (A) 2 Hz,(B) 4 Hz, (C) 5 Hz, (D) 6 Hz and (E) 7 Hz.
(C) 8 Hz and (D) 16 Hz were prepared and tested. When vertical stripes were used as the mask image, significant differences from the stationary illusion image were observed at all frequencies (Table 4-3). In the case of horizontal stripes, significant differences were observed at 8 Hz and 16 Hz (Table 4-4). Significant differences between the vertical and horizontal stripes were only observed when the drift frequency was 4 Hz (Table 4-5)

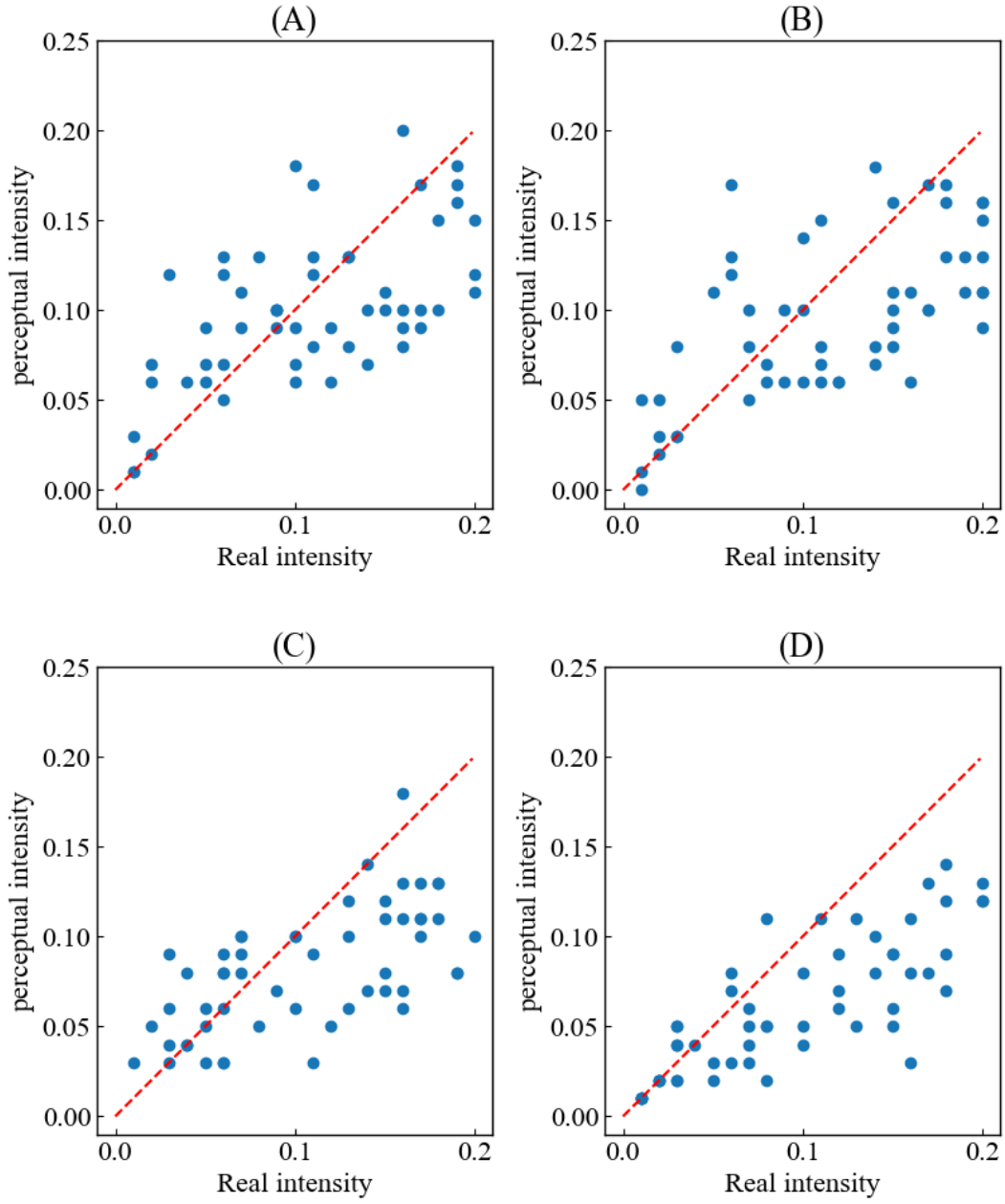

Fig. 4-6 Experimental results when the mask image of the vertical stripes is shifted in time. Mask image frequencies (A) 2 Hz (B) 4 Hz, (C) 8 Hz and (D) 16 Hz.

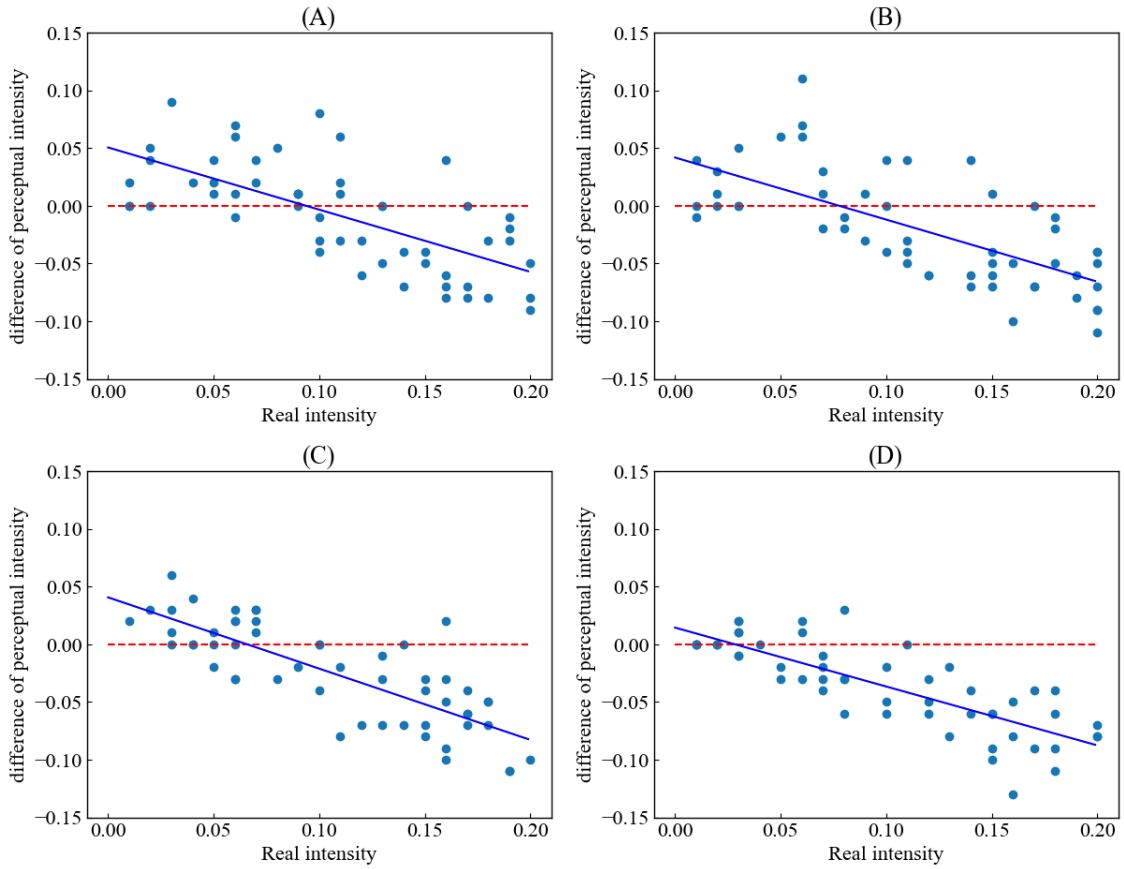

Figure 4-7. Graphs with the vertical axis of the graph in Figure 4-6 changed to the difference from the horizontal axis.(A) 2 Hz,(B) 4 Hz, (C) (C) 8 Hz,(D) 16 Hz.

Table 4-3 Results of t-tests between static and drift illusion images (vertical stripes) Significance level 0.05

Time-frequency	fp value
2 Hz	0.002
4 Hz	4.69e-05
8 Hz	4.22e-06
16 Hz	2.07e-08

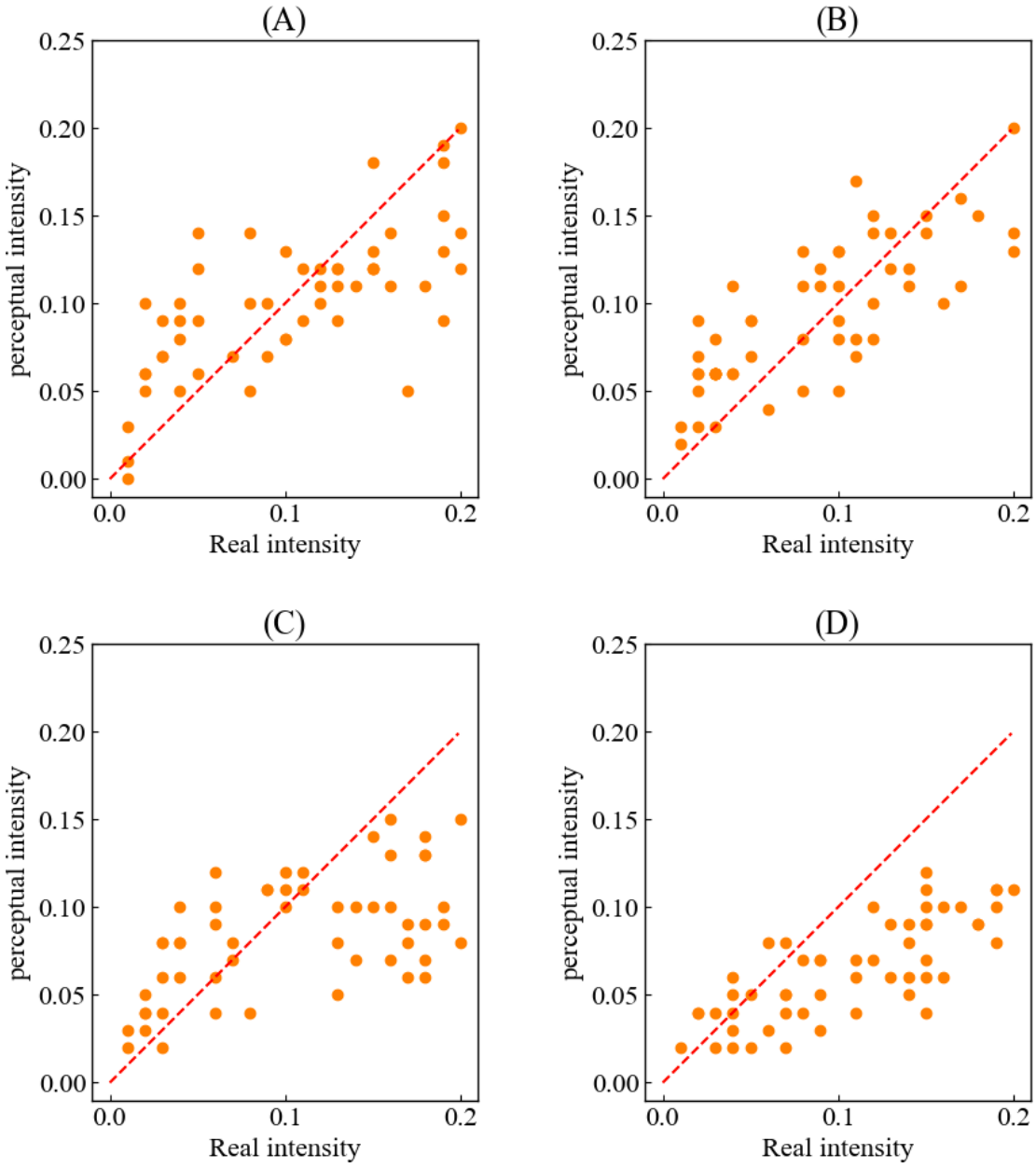

Figure 4-8 Experimental results when the mask image of the horizontal stripe is shifted in time.(A) 2 Hz,(B) 4 Hz,(C) 8 Hz and(D) 16 Hz.

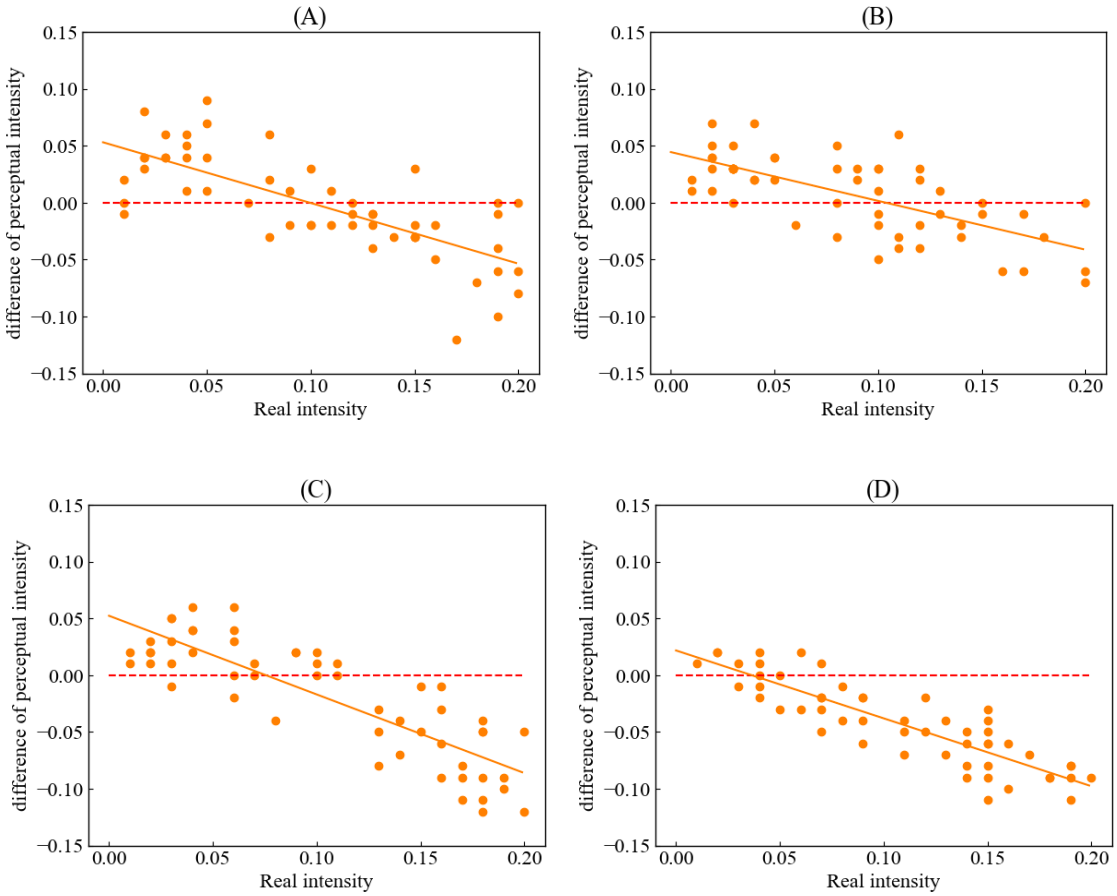

Figure 4-9. Graphs with the vertical axis of the graph in Figure 4-8 changed to the difference from the horizontal axis.(A) 2 Hz,(B) 4 Hz, .

(C) 8 Hz,(D) 16 Hz.

Table 4-4 Results of t-tests between static and drift illusion images (horizontal stripes)

Time-frequency	fp value
2 Hz	0.22
4 Hz	0.82
8 Hz	0.003
16 Hz	8.05e-09

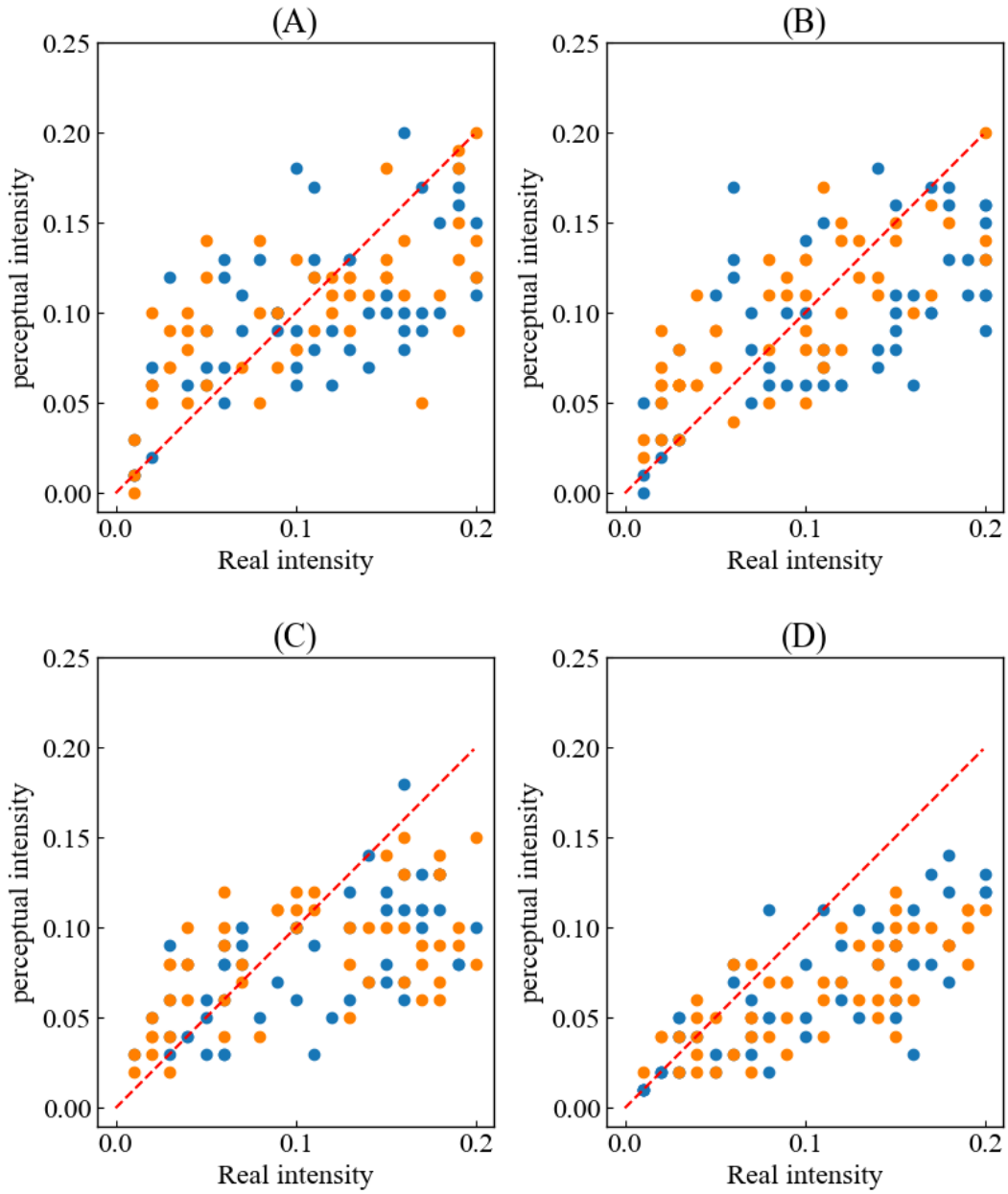

Figure 4-10 Overlaid graphs of Figures 4-6 and 4-8. (A) 2 Hz (B) 4 Hz (C) 8 Hz (D) 16 Hz. for both vertical (blue) and horizontal (orange) stripes, the illusion effect decreases as the temporal frequency of the mask image drift increases.

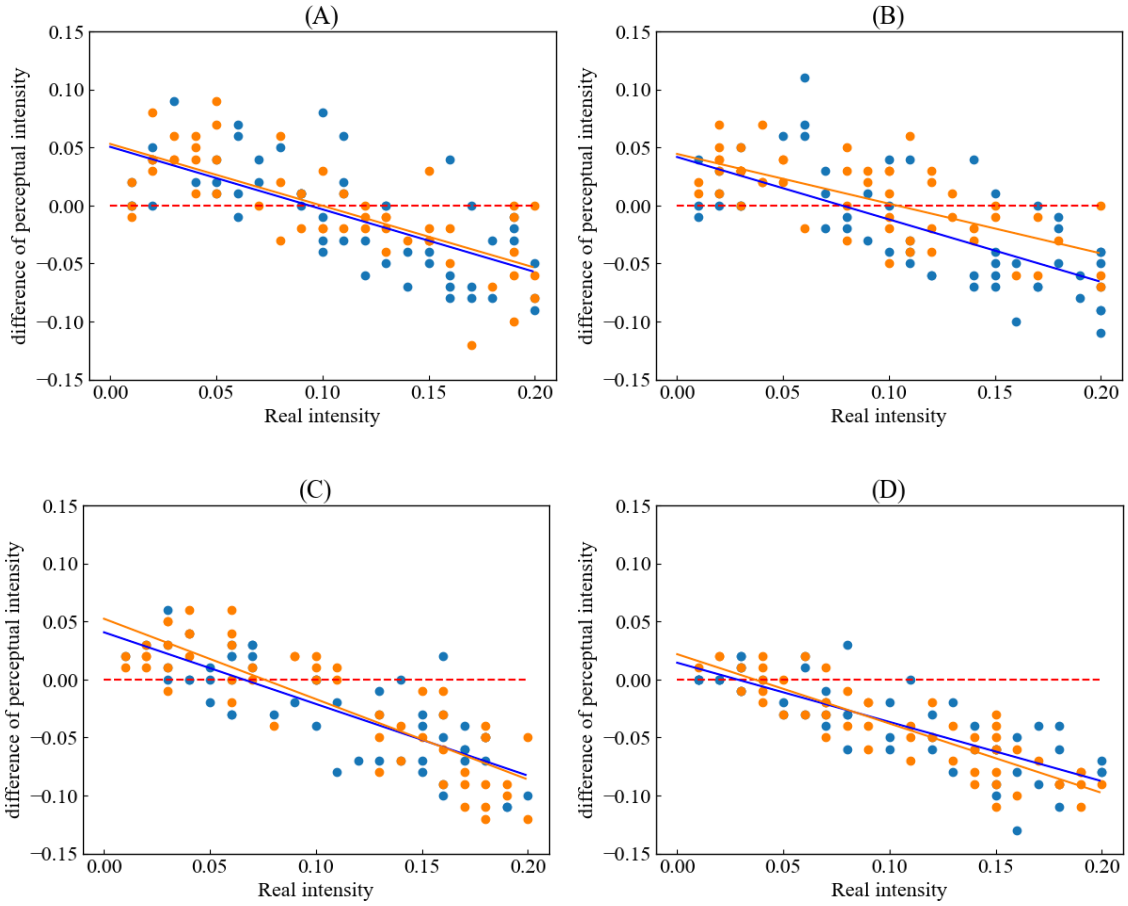

Figure 4-11 Vertical axis of the graph in Figure 4-10 as a difference from the horizontal axis.(a) 2 Hz,(b) 4 Hz,(c) 8 Hz,(d) 16 Hz.

Table 4-5 Results of t-tests between drift illusion images of vertical and horizontal stripes. Significance level 0.05

Time-frequency	fp value
2 Hz	0.48
4 Hz	0.001
8 Hz	0.56
16 Hz	0.32

4.2.2 Illusion effect by single oscillating illusion images.

The experimental results when the whole illusory image is changed with time are shown below. Figure 4-12 shows the results of the experiment in which the entire illusory image of vertical and horizontal stripes was subjected to sin(2t), sin(4t), sin(8t) and sin(16t) single oscillations in two directions (horizontal and vertical). The respective movement periods are shown in Fig. 4-12, with the periods becoming shorter in the order from (A) to (D).
Figure 4-13. In Fig. 4-12, it is difficult to understand the change of the illusion effect by the change of the period, but Fig. 4-13 shows that the four approximate lines are divided into two parts, the upper and lower parts. In Figures 4-14 and 4-15, the results are plotted for each mask image (vertical and horizontal stripes) and direction of movement (vertical and horizontal). Figures 4-14 and 4-15 show that when the mask image is a vertical stripe, the illusion effect decreases when the illusion image is moved horizontally in a single oscillation, and when the mask image is a horizontal stripe, the illusion effect decreases when the mask image is moved vertically in a single oscillation. The common point among them is that the direction of the stripes of the high-spatial frequency component of the mask image and the direction of movement are orthogonally related. Furthermore, t-tests were conducted between the stationary and single-vibration illusion images. Significant differences were found between the vertical stripes and the stationary illusion image at all frequencies when the vertical stripes were subjected to a single oscillation in the horizontal direction (Table 4-6) When the horizontal stripes were single-vibrated in the vertical direction, significant differences were found at all frequencies between the horizontal stripes and the stationary illusion image (Table 4-9) When stripes in the mask image was parallel to the direction of the single oscillation, no significant differences were found at all frequencies (Tables 4-7 and 4-8)

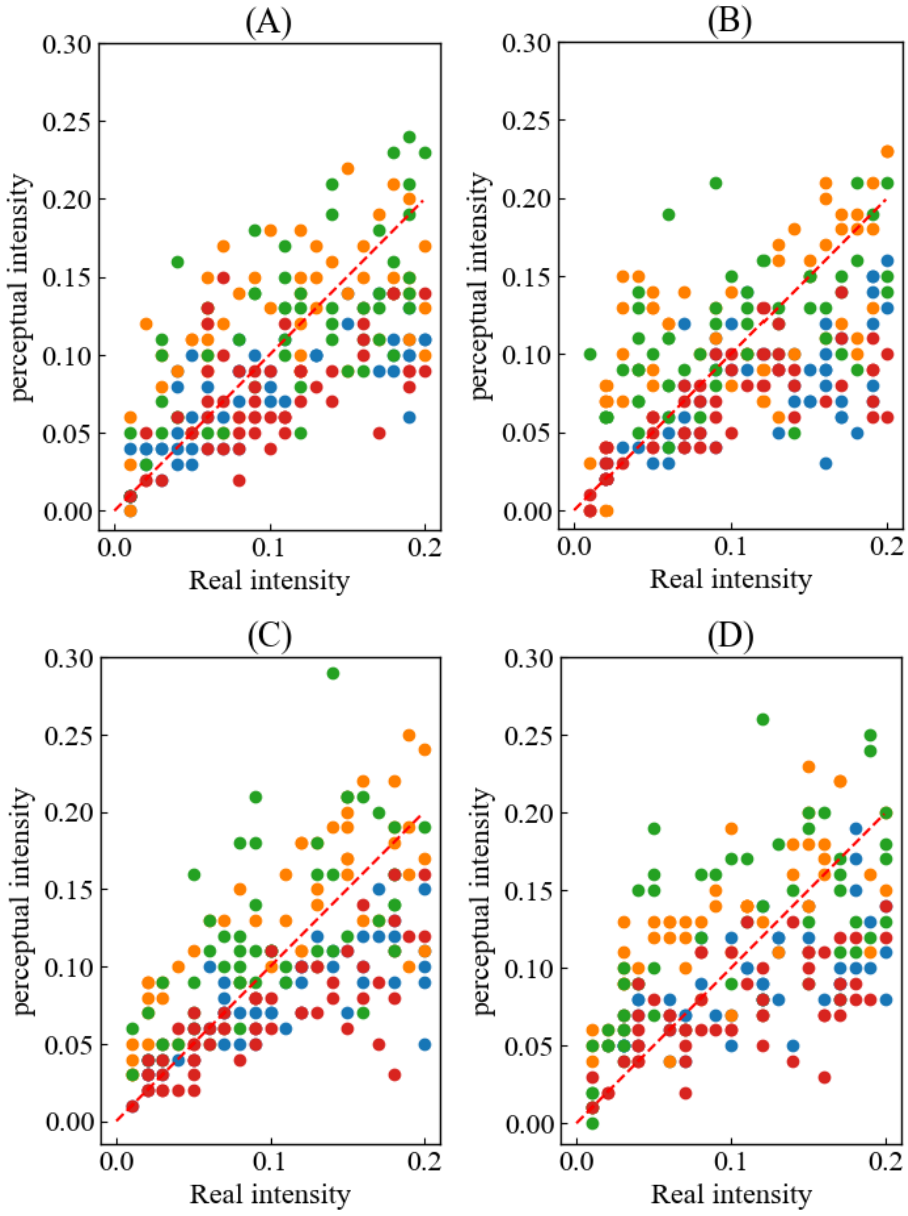

Figure 4-12 Experimental results of single oscillation of the whole illusion image at each period. Frequencies of single oscillation are (A) $f = 2/\pi$, (B) $f = 4/\pi$, (C) $f = 8/\pi$ and (D) $f = 16/\pi$, respectively; each plot in the figure shows the vertical shift of vertical stripes (blue), horizontal shift of vertical stripes (orange), vertical shift of horizontal stripes (green) and horizontal shift of horizontal stripes (red).

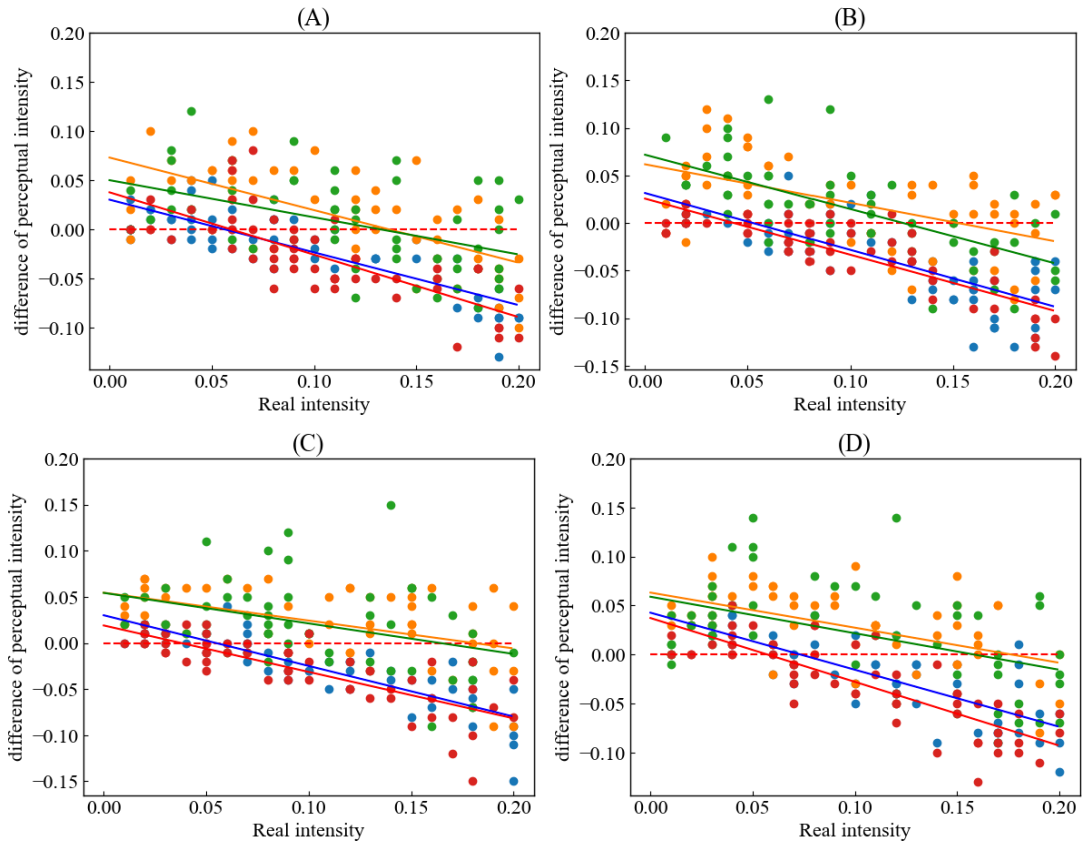

Figure 4-13 The vertical axis of the graph in Figure 4-12 is the difference from the horizontal axis. It can be read that the illusion effect decreases when the mask image (vertical or horizontal stripes) and the direction of movement (vertical or horizontal movement) are orthogonal.

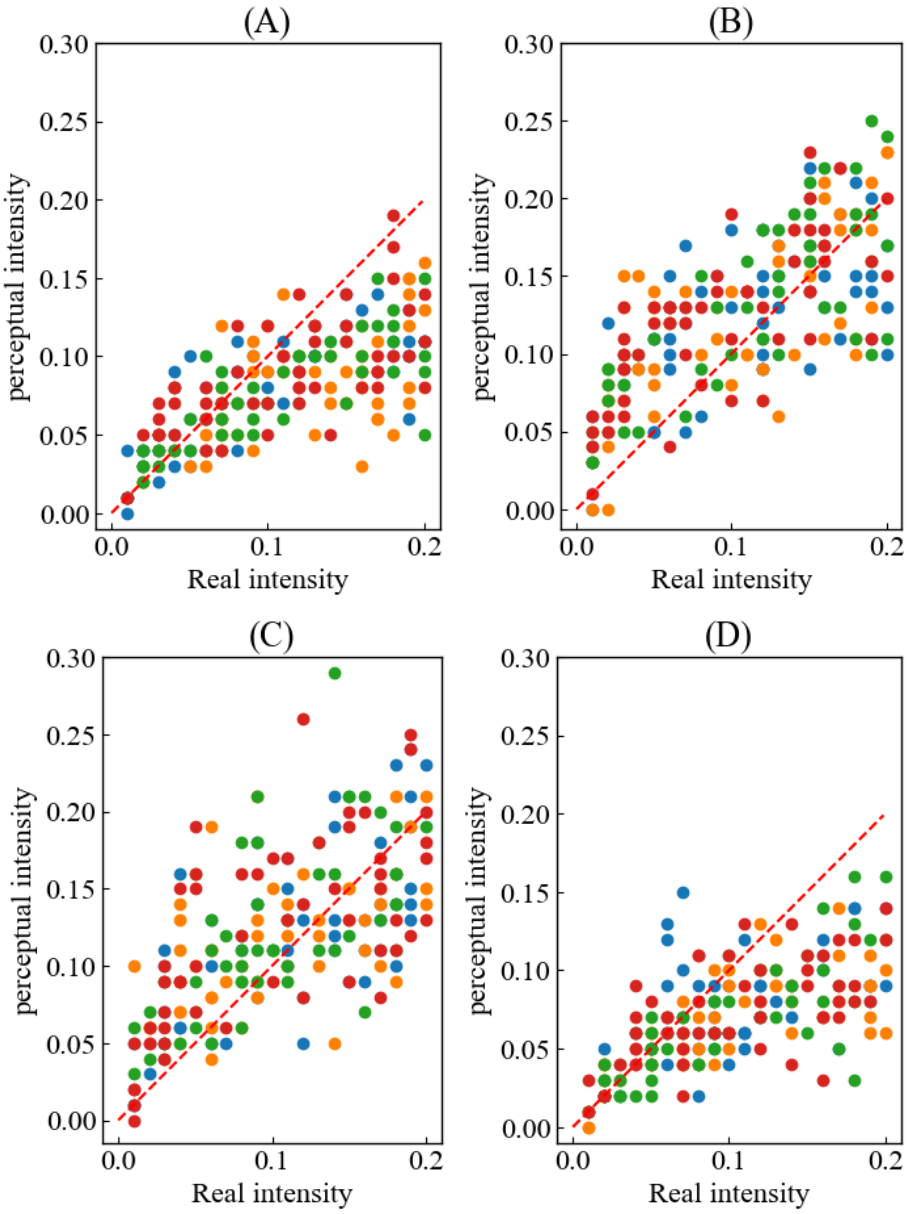

Figure 4-14 Results for each mask image (vertical stripe, horizontal stripe) and movement direction (vertical movement, horizontal movement). (A) Horizontal shift of vertical stripes, (B) vertical shift of vertical stripes, (C) horizontal shift of horizontal stripes, (D) vertical shift of horizontal stripes. The plots in each graph are colour-coded according to the frequency of the illusion image, showing (blue) $f = 2/\pi$, (orange) $f = 4/\pi$, (green) $f = 8/\pi$ and (red) $f = 16/\pi$.

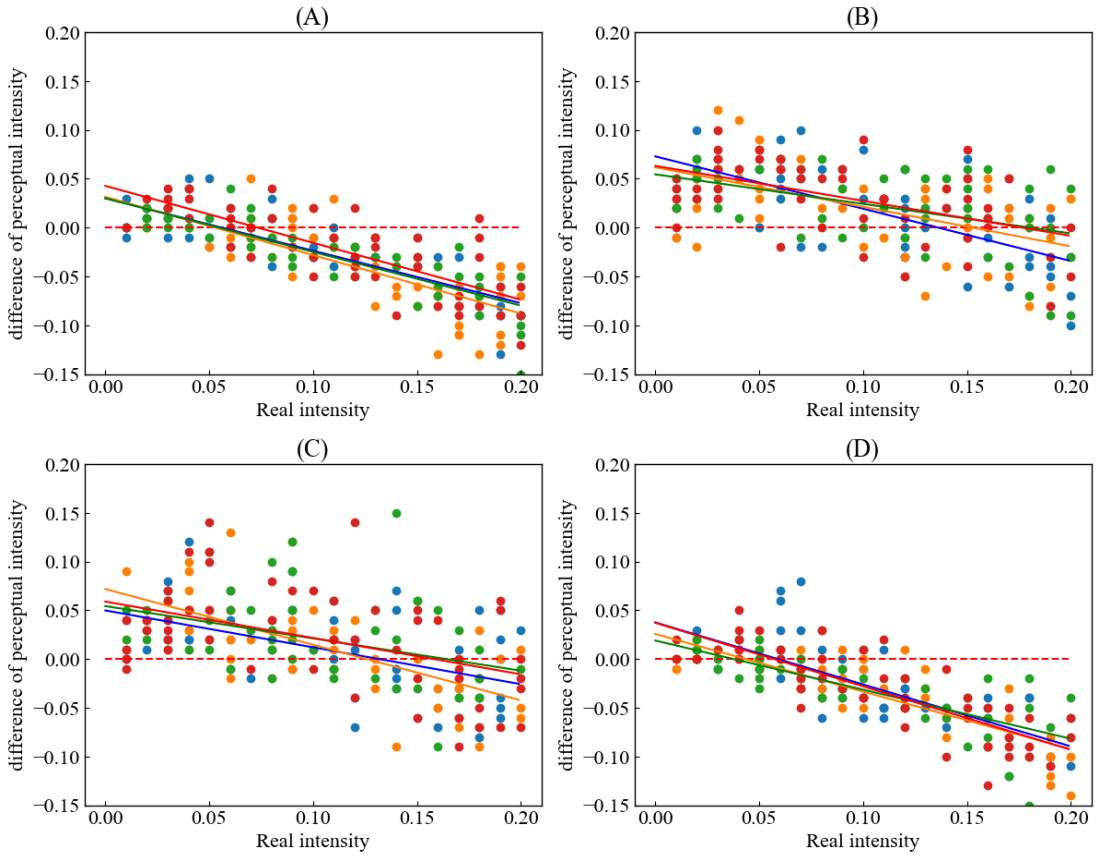

Figure 4-15 The vertical axis of the graph in Figure 4-14 is the difference between the horizontal axis and. (a) horizontal shift of vertical stripes,(b) vertical shift of vertical stripes,(c) horizontal shift of horizontal stripes,(d) vertical shift of horizontal stripes. The plots in each graph are colour-coded for each frequency of the illusion image, showing (blue) $f = 2/\pi$,(orange) $f = 4/\pi$,(green) $f = 8/\pi$ and(red) $f = 16/\pi$. Approximate straight lines are drawn for each colour.

Table 4-6. Results of t-tests between illusion images of the static illusion and the horizontal single oscillation illusion (vertical stripes)

Significance level 0.05

Time-frequency	fp value
2/π Hz	2.327e-05
4/π Hz	7.108e-09
8/π Hz	5.596e-07
16/π Hz	1.485e-05

Table 4-7. Results of t-tests between illusion images of the static illusion and the longitudinal single oscillation illusion (vertical stripes).

Significance level 0.05

Time Frequency f	p-value
2/π Hz	0.365
4/π Hz	0.732
8/π Hz	0.850
16/π Hz	0.567

Table 4-8. Results of t-tests between the static and lateral single oscillation illusion images (horizontal stripes).

Significance level 0.05

Time Frequency f	p-value
2/π Hz	0.7882
4/π Hz	0.5020
8/π Hz	0.1786
16/π Hz	0.1790

Table 4-9. Results of t-tests between illusion images of the static illusion and the longitudinal single oscillation illusion (horizontal stripes)

Significance level 0.05

Time-frequency	fp value
2/π Hz	9.030e-05
4/π Hz	4.674e-06
8/π Hz	9.946e-06
16/π Hz	2.677e-05

4.3 consideration

From Sections 4.1 and 4.2, the illusory effect of the illusion image decreased when the viewing distance was increased, when the mask image of the illusion image was made to drift, and when the illusion image was made to oscillate perpendicularly to the mask image in the illusion image. When the viewing distance of the illusory image was converted into the visual angle, the visual angle was 9.147° at an observation distance of 50 cm and 4.581° at 100 cm. The spatial frequency of the mask image at an observation distance of 50 cm is 80 cycles/9.147 degrees = 8.746 cpd and that at 100 cm is 80 cycles/4.581 degrees = 17.49 cpd. The contrast sensitivity of the human eye is known to reach its maximum value around 10 cpd, as described in section 2.4, so it can be assumed that the 50 cm viewing distance is more affected by the contrast of the stripes in the mask image. The high contrast sensitivity at an observation distance of 50 cm is also considered to be a strong effect of lateral inhibition. Lateral inhibition refers to the inhibition of the neuronal activity of other neurons in the periphery, which are less responsive to sensory stimuli, by neurons that respond to sensory stimuli in the centre of the receptive field via surrounding inhibitory neurons (Barlow, 1953; Barlow, 1953). (Barlow,1953)

(Lateral suppression in the retina has been reported by (Kuffler, 1953) et al. In section 4.2, the illusion effect was reduced by physically moving the illusion image. First, in section 4.2.1, the mask image was drifted. The illusion effect was reduced by the drift of the mask image for both vertical and horizontal stripes. Also. In section 4.2.2, the illusion effect was reduced when the whole illusion image was subjected to a single vibration in the direction orthogonal to the direction of the stripes in the mask image. The common feature of both operations is that the spatial frequency in the illusory image perceived by the subject is perceived to be higher than it actually is (Fig. 4-16). (Fig. 4-16) Thus, it is considered that this temporary perception due to the drift of the mask image cancelled the effect of the aforementioned lateral suppression, and as a result, the illusion effect was reduced. In other words, this result suggests that the spatial frequency of the mask image is a major factor in the disappearance illusion.

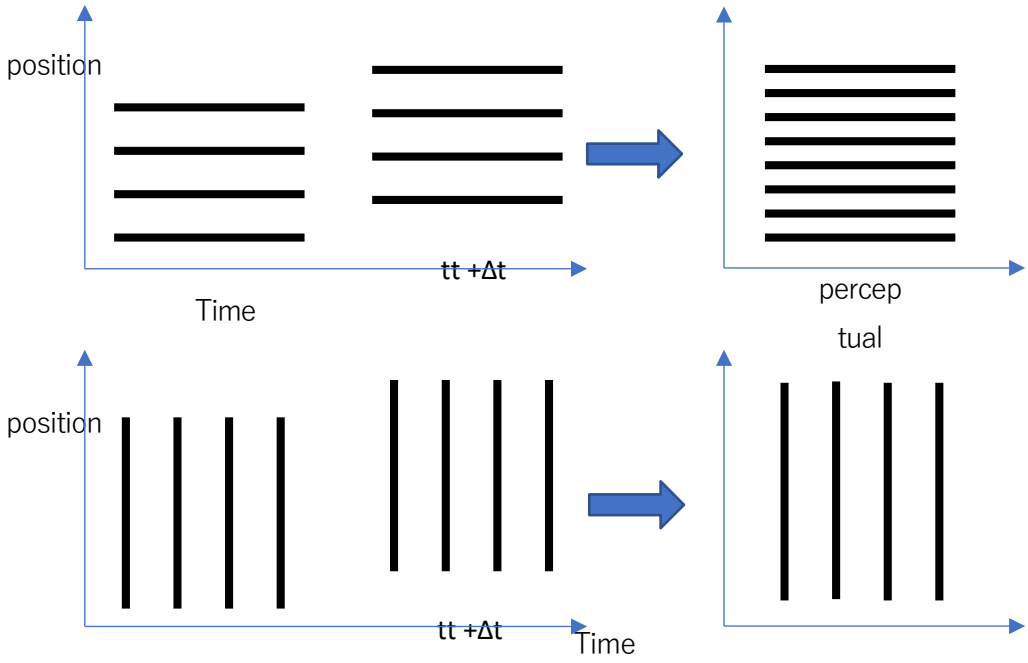

Figure 4-16 Integration of temporal information on perception. When the relationship is orthogonal to the direction of the stripes, the spatial frequency is perceived to have increased (top figure). On the other hand, when the direction of movement coincides with the direction of the stripes, the perceived spatial frequency does not change (bottom figure).

5 Chapter　Neural circuit simulation

5.1　Hodgkin-Huxley Model (HH Model)

Neural circuit simulation is the numerical simulation of the behaviour of neural circuits in the brain on a computer. At present, the algorithms of information processing in the whole brain have not yet been elucidated and there are many unknowns. However, when it comes to the single neurons that make up the brain, numerous studies have been conducted and their behaviour can be specifically described by differential equations. Since differential equations can be solved numerically using computers, the programmes can be used to reproduce the human brain on a supercomputer.

The world's first mathematical model of a single neuron was formulated by Alan L. Hodgkin and Andrew F. Huxley in 1952; Hodgkin and Huxley found that the action potential of a neuron is generated by transient changes in cell membrane permeability to sodium (Na^+) and potassium ions (K^+) They found that this is caused by changes They then analysed the electrical properties of the plasma membrane and proposed the Hodgkin-Huxley model (hereafter HH model). This HH model is the basis of all neuronal models and is expressed by the following equation (Gerstner, W & Kistler 2002) (Hodgkin
A. & Huxley A. 1952)

$$C\frac{dV}{dt} = g_{!"\#\$}(V(t) - E_{\%\&'(}) - g_{)\#}(V,t)(V(t) - E_{*'}) - g_{+}(V,t)(V(t) - E_{+}) + I_{\&,-}(t) \quad (5.1)$$

C is the capacitance of the membrane [μF/cm^2]. t is the time [ms]. $V(t)$ is the membrane potential [mV]. $\bar{g}_{!"\#\$}$ is the leakage conductance [mS/cm^2]. Here, conductance is the reciprocal of resistance [Ω] and represents the ease of current flow. $E_{\%\&'(}$ is the reversal potential of Cl^- ions [mV]. $g_{)\#}(V, t)$ is the potential dependent Na^+ channel conductance [mS/cm^2]. $E_{*'}$ is the reversal potential of Na^+ ions [mV]. $g_{+}(V, t)$ is the potential dependent K^+channel conductance [mS/cm^2]. E_+ is the reversal potential of K^+ ions [mV]. $I_{\&,-}(t)$ is the external current injected from outside the cell [μA/cm^2]. Note that these values are normalised per unit area because the total capacitance of the capacitor and the number of channels that determine the conductance value are proportional to the membrane area. To summarise the values of the constants in

the equations, C

= 1 μF/cm^2 and normalised to $g_{!"\#\$}$ = 0.3 mS/cm^2 , $E_{*\cdot(}$ = 10.6 mV, $g_{)\#}$ = 120 mS/cm^2

$E_{*\cdot}$ = 115 mV, $g_{\_}$ = 36 mS/cm^2 and E_+ = -12 mV.

Also, the Na^+ conductance $g_{)\#}(V, t)$ and K^+ conductance $g_{\_}(V, t)$ in the equation are respectively

Expressed by the formula.

$$)\#g\ (V,t) = \bar{g}_{*\cdot}\, m/\ (V,t)h(V,t) \qquad (5.2)$$
$$\_g\,(V,t) = g_{+}\, n^{0}\ (V,t)$$

Note that these vary with time, where $\bar{g}_{*\cdot}$ and $\bar{g}_{+}$ are constant and maximum conductance [mS/cm^2] respectively. $m(V,\ t)$, $h(V,\ t)$ and $n(V,\ t)$ in the equations are gate variables that depend on membrane potential V, respectively. The gate variables represent the aperture of the ion channel and are updated by the following equation.

$$\frac{dm}{dt} = \alpha_{1}(V)\mathrm{D1} - m(V,t)\mathrm{E} - \beta_{1}(V)m(V,t) \qquad (5.3)$$
$$\frac{dh}{dt} = \alpha_{2}(V)\mathrm{D1} - h(V,t)\mathrm{E} - \beta_{2}(V)h(V,t)$$
$$\frac{dn}{dt} = \alpha_{3}(V)\mathrm{D1} - n(V,t)\mathrm{E} - \beta_{3}(V)n(V,t)$$

In the above equations $\alpha_4\ (V)$ and $\beta_4\ (V)$ (x represents m, h and n) are defined by the following equations, respectively. m is the activation parameter of the Na^+ conductance, h is the inactivation parameter of the Na^+ conductance and n is the activation parameter of the K^+ conductance. Note that these parameters are values based on experiments with giant axons of the Yari squid.

$$\alpha_1(V) =. \frac{2.5 - 0.1V}{\exp(2.5 - 0.1V) - 1} \qquad (5.4)$$

$$\beta_1(V) = 4\exp\ \mathrm{K}\text{-}\frac{V}{18}\mathrm{M}$$

$$\alpha_2(V) = 0.07\exp\ \mathrm{K}\text{-}\frac{V}{20}\mathrm{M}$$

$$\beta_2(V) =. \frac{1}{\exp(3 - 0.1V) + 1}$$

$$\alpha_3(V) = \frac{0.1 - 0.01V}{\exp(1 - 0.1V) - 1}$$

$$\beta_3(V) = 0.125\exp\ \mathrm{K}\text{-}\frac{V}{80}\mathrm{M}$$

Thus, the HH model is a non-linear dynamical system consisting of four variables $V(t)$, $m(V,\ t)$, $h(V,\ t)$ and $n(V,\ t)$, and by solving these differential equations the behaviour of the neurons can be reproduced on the computer.

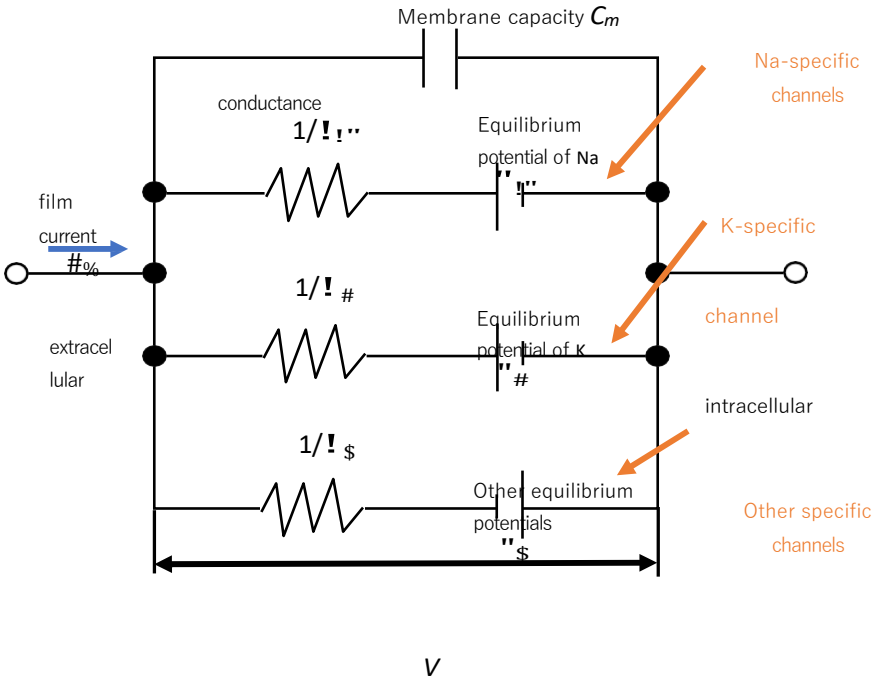

Figure 5-1. Equivalent circuit model of the cell membrane in the HH model (Hodgkin A. & Huxley A. 1952) In the parallel equivalent circuit model of the cell membrane, the cell membrane of the neuron is replaced by a capacitor and the ion channels embedded in the cell membrane by a variable resistance. Ion channels are a type of membrane transporter that selectively allows certain ions to pass through. For each type of ion, there are different ion channels. Ion channels also have different conductances and equilibrium potentials, depending on the type of ion. in the HH model, Na^+ channels, K^+ channels and other ion channels are assumed. The other ion channels are channels that could not be identified in 1952. It should be noted that most of these are now known to be Cl^- channels.

5.2 Integral firing model (LIF model)

Section 5.1 described the HH model, the first model of a single neuron. In this paper, we describe a simpler form of the model than the HH model, the Leaky Integrate-and-fire (LIF) model, which has only one variable as a parameter and is described by the following equation

$$\tau \frac{dv}{dt} = -(v(t) - V_{5\&6-}) + R_{\&,-}(t) \tag{5.5}$$

$$v(t) > \theta \Longrightarrow S(t) = 1, v(t) \leftarrow V_{7"8"9}$$

$$v(0) = V_{:3:9}$$

Where $v(t)$ [mV] is the membrane potential at a time t. τ[ms] is the time constant of the membrane potential. $V_{7"89}$ $[mV]$ is the resting potential. R[MΩ] is the membrane resistance. $I_{"49}$ $(t)[nA]$ is the current flowing from the cell exterior at a time t. θ[mV] is the threshold value. $V_{7"8"9}$ [mV] is the reset potential. The initial potential is given by $V_{:3:9}$ [mV] In the LIF model, when $v(t)$ exceeds the threshold value θ, depolarisation occurs and the membrane potential increases and fires. After firing, it is assumed that repolarisation occurs and the membrane potential decreases to the reset potential $V_{7"8"9}$. Thus, compared to the HH model equation with four variables $V(t)$, $m(V, t)$, $h(V, t)$ and $n(V, t)$, the LIF model has a simpler expression with only membrane potential $v(t)$. Note that in the LIF model, synapses are also current-based synapses in sets with neurons in the current-based model. In the current-based synapse, the synaptic current $g_{8;3}$ (t) is used directly as the synaptic current. Note that a current-based model is a model in which the conductance $g(V,t)$ is not explicitly described.

$$_{8;3}I\ (t) = w \cdot g_{8;3}\ (t) \tag{5.6}$$

The coupling strength is denoted *by w, with* positive values *of w* indicating excitatory coupling and negative values indicating inhibitory coupling. In the present study, simulations were performed using neurons of this LIF model and current-based synapses.

5.3 ON Central retinal receptive field model

The bipolar cells that receive input from photoreceptor cells, as well as retinal neurons and lateral optic tectal knee cells, have an ON-centre OFF-periphery type that responds excitably when bright light is received in the centre of the receptive field and inhibitory when bright light is received in the periphery, and an ON-centre ON-periphery type that responds inhibitively when bright light is received in the centre and excitably when bright light is received in the periphery. OFF-centre ON-periphery type exists (Kuffeler, S.W. 1953) As the central and peripheral parts of both types are concentrically arranged and show opposite responses, this receptive field is called the centre-periphery antagonistic receptive field. The central-peripheral antagonistic receptive field can be divided into excitatory and inhibitory responses depending on how the contrast stimulus is projected to the central and peripheral areas, so it can be said to transmit information on the width and location of light/dark contrast. In the visual cortex, in particular, in addition to the receptive fields described above, there are also simple-type cells that recognise line segments with a specific position and slope, and complex-type cells that recognise line segments with a specific slope regardless of their position (Hubel, D. & Wiesel, T. 1962).

It is also known that the model of the peri-centre antagonistic receptive field can be represented by the difference of two Gaussian functions (Rodieck, R. 1965) In the present study, therefore, the coupling strength of horizontal coupling was assumed to be stochastically determined according to the distance between neurons, with a Mexican hat-shaped function with excitatory coupling dominance for short distances and inhibitory coupling dominance for long distances. (Figure 5-2: light blue solid line)

$$I(i,j) = k_< \exp\left(\frac{-|i-j|^=}{2\sigma_<^=}\right) - k_= \exp\left(\frac{-|i-j|^=}{2\sigma_=^=}\right) \qquad (5.7)$$

In the equation $i - j$ is the distance between two neurons i and j in the two-dimensional plane. Figure 5-2 illustrates the above equation. The vertical axis is the coupling strength and the horizontal axis is the distance between the neurons. The red and blue wavy lines represent the coupling strength between excitatory and inhibitory neurons. The width of the inhibitory coupling is wider than the

excitatory coupling, as the coupling through the inhibitory neuron reaches farther. In the light blue solid line, the area where the coupling strength is negative means that the inhibitory input is indirectly provided via the inhibitory neurons. The simulation in this study is a simplified one. When the illusion is observed at a distance, the excitatory coupling is assumed to be at $\mathbf{r}^{+}$ of the Mexican hat-shaped model, and when the illusion is observed at close range, the inhibitory coupling is assumed to be outside $\mathbf{r}^{+}$.

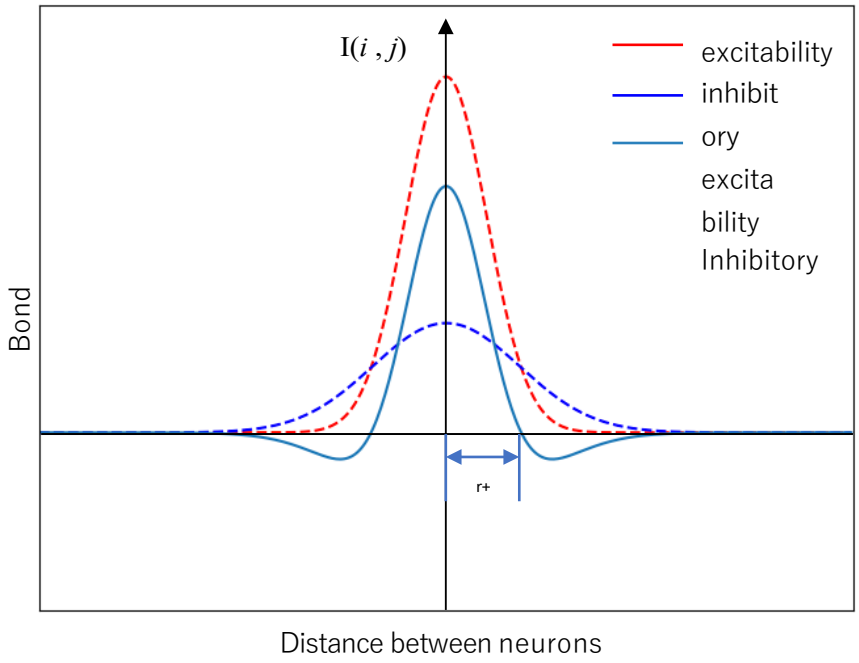

Figure 5-2 Shape of horizontal connections of neurons. The vertical axis represents the coupling strength and the horizontal axis represents the distance between neurons. The width of inhibitory connections is wider than that of excitatory connections, as it is considered that connections reach farther through inhibitory neurons than between excitatory neurons.

6 Chapter Simulation results and solutions Analysis

6.1 Simulation results

Assuming the model shown in Figure 5-2, the results of the neuron firing simulation are

The following are shown. The LIF model (Section 5.2) was adopted for the neurons.

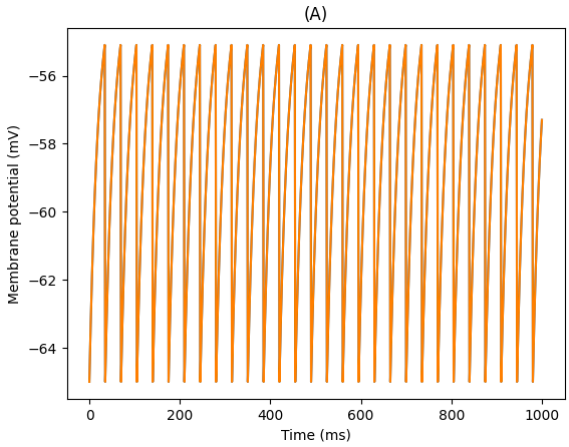

FIGURE 6-1 Plot of membrane potentials of two non-synaptically coupled neurons. Simulated conditions with only the text image observed without the mask image. Firing rate: 28 Hz.

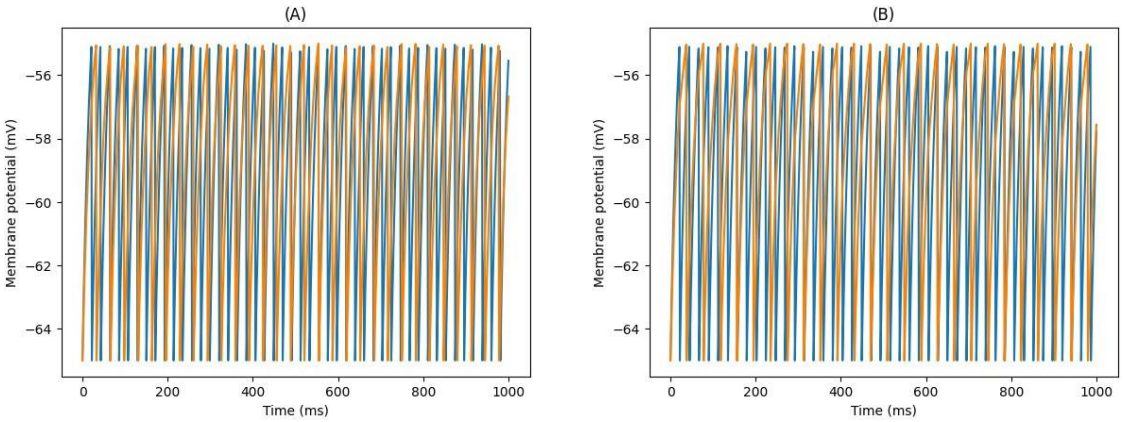

Figure 6-2 Plot of membrane potentials when two neurons are coupled at a current-based exponential decay synapse. (A) Excitatory coupling dominance. Simulated when the illusion is observed from a distance (observation distance 100 cm). Firing rate: 30 Hz.(B) For inhibitory coupling dominance.

Simulation when the illusion is observed from a short distance (observation distance 50 cm). Firing rate:.
25 Hz.

6.2 consideration

Figure 6-1 shows a simulation of the firing of two neurons in an independent state in which they are not connected to each other by synapses. It reproduces a situation in which only the text image, excluding the mask image, is observed, not the illusory image. The firing rate was 28 Hz. Figure 6-2 (a) reproduces the situation when the illusion was observed from a distance (100 cm). The coupling strength w was set to a positive value, reproducing the situation of excitatory coupling dominance. On the other hand, Fig. 6-2 (B) shows the reproduction of the illusion observed from a short distance (50 cm). The coupling strength w was set to a negative value, reproducing the situation of inhibitory coupling dominance. Comparing the firing rates of the two, the firing rate in Fig. 6-2(A) was 30 Hz, whereas in Fig. 6-2(B) it was 25 Hz. This compares to 28 Hz in the situation without synaptic coupling, where the firing rate of 30 Hz in Fig. 6-2(A) was higher than the simulation result of 28 Hz in Fig. 6-1, while the firing rate of 25 Hz in Fig. 6-2(B) was lower than that of 28 Hz. This is consistent with the results of Experiment 1-2 (section 4.1.2). Therefore, it can be said that the present simulation was able to qualitatively reproduce the behaviour of the firing of neurons in the retinal receptive field when the distance of the illusory image was varied and observed, albeit in a simplified manner.

7 Chapter conclusion Theory

In this study, quantitative measurement of the illusion effect in disappearing illusion figures and analysis of the results were conducted in Chapter 4, and simulation of the firing of neurons in the retinal receptive field model during observation of illusion figures was conducted in Chapter 6. in Section 4.1.1, a disappearing illusion was created using five types of mask images with high spatial frequency, and the mask The illusion effect was measured for each mask image. In all mask images, the illusion was generally observed when the opacity was less than 0.1. The problem is that the shapes of mask images (D) and (E) are different from those of the other three mask images due to the specification of PsychoPy. In the future, it will be necessary to consider other mask creation methods and conduct experiments in which the shapes of the mask images to be compared are all the same.

In section 4.1.2, two patterns of observation distances were prepared: 50 cm (visual angle: 9.147°) and 100 cm (visual angle: 4.581°), and the illusion effect at each observation distance was compared. As a result, the illusion effect was reduced at an observation distance of 100 cm compared to that at an observation distance of 50 cm for each mask image. A t-test was conducted, and significance was also found between the two groups. The problem is that only two observation distances were used. In the future, it is necessary to consider the correspondence between the continuous change in the observation distance and the illusion effect by increasing the observation distance. In addition, we would like to measure the illusion effect when the spatial frequency of the mask image is continuously changed without changing the observation distance.

4.2.1 In Section 3.2, the illusion effect during the drift of the mask image in two directions, vertical and horizontal, was measured. As a result, as the time frequency of the drift of the mask image in the vertical and horizontal stripes increased, the illusion effect increased accordingly. A t-test was conducted, and the difference from the static illusion image was observed at time frequencies of 4 Hz and above, except at 2 Hz.

4.2.2 In Section 3.2.2, the entire illusory image of vertical and horizontal stripes is shown as sin(2t),sin(4t),sin(8t) and sin(8t) in two directions (horizontal and vertical).

Single oscillation with sin(16t). As a result, Figures 4-12 and 4-14 were obtained. In Figure 4-12, the single vibration

The results were summarised for each frequency of movement, and in Figure 4-14,

the results were summarised for each mask image and movement direction. Figures 4-14 and 4-15 confirm that the illusion effect is reduced when the direction of the stripe of the high spatial frequency component of the mask image and the direction of movement are in an orthogonal relationship. The problem in the experiments conducted in Sections 4.2.1 and 4.2.2 is that the temporal frequencies of the drift and single oscillation of the mask image and the entire illusory image in both experiments are not consistent. In the future, it will be possible to compare the illusion effects between Sections 4.2.1 and 4.2.2 by aligning the time frequencies of the drift and single oscillation. In addition, the time-frequency should be varied continuously so that the time-frequency and the illusion effect can be described in a more relevant way. The overall experimental results suggest that the spatial frequency of the mask image is a major factor in the disappearing illusion.

In Chapter 6, we considered an ON-centred receptive field model and simulated the firing of neurons during observation of an optical illusion. Three patterns were considered: when only the text image was observed, when the illusory image was observed from a distance (100 cm) and when the illusory image was observed from a short distance (50 cm).

The simulation results, which are simple but consistent with the experimental results, were successfully obtained by simulating the coupling strength at different levels.

8 Chapter reference text Dedication

Arai H, Arai S , "Mathematical models of vision and structure analysis of visual illusions", Japanese Psychological Review ,Vol. 55, No. 3, 2012,pp.309-333.

Barlow HB. Summation and inhibition in the frog's retina.*J Physiol (Lond)* ,1953;119:pp.69-88.

C. Blakemore, F. W. Campbell, "On the existence of neurons in the human visual syste m selectively sensitive to the orientation and size of retinal images", *The Journal of Physiology*, Volume 203, Issue 1,1969,pp.237-260.

Christina Enroth-Cugell, J. G. Robson, "The contrast sensitivity of retinal ganglion cells of the cat", *The Journal of Physiology*, Vol. 187, Issue 3,1966,pp.517-552.

David H.Foster, "Colour constancy", *Vision Research*, Vol51,Issue7,2011,pp.674-700.

Gerstner W and Kistler M, "Spiking Neuron Models", *Cambridge University press*, 2002.

Hodgkin, A. L., and Huxley, A. F., A "quantitative description of membrane current and its application to conduction and excitation in the nerve. "*Journal of Physiolo gy*,117(4),1952,pp.500-544, https://www.ncbi. nlm.nih.gov/pmc/articles/PMC1392413/pdf/jp hysio101442-0106.pdf (last accessed 24/01/2023).

Hubel, D. H., & Wiesel, T. N., "Receptive fields, binocular interaction and functional arc hitecture in the cat's visual cortex. "*Journal of Physiology (London),160*(1),1962,pp.106 -154.

Hybrid Images,@MIT, http://olivalab.mit.edu/hybrid_gallery/gallery.html (last accessed 24/01/2023)

J.G. Robson, "Spatial and Temporal Contrast-Sensitivity Functions of the Visual System", *Journal of the Optical Society of America*, Vol.56, Issue 8,1966,pp.1141-1142

J.MASON, P.KASZOR, C.BOURASSA , "Perceptual Structure of the Necker Cube", *NATURE* ,Vol.244,1973,pp.54-56.

Kuffeler,S.W, "Discharge patterns and functional organisation of the mammalian retina.", *Jour nal of neurophysiology*,16(1),1953,pp.37-68.

Monge, Gaspard. "Mémoire sur quelques phénomènes de la vision. "*Annales de Chimie*. Vol. 3,1789

Murakami I, "Visual Illusions as Tools for Vision Research", Japanese journal of optics. : publication of the Optical Society of Japan 39(2), 2010,pp.66-74.

Nicola Bruno, Volker H. Franz, "When is grasping affected by the Müller-Lyer illusion?" A quantitative review, *Neuropsychologia* ,Vol. 47, Issue 6, 2009, pp. 1421-1433.

Oliva, A., Torralba, A. and Schyns, P.G., "Hybrid Images". ACM Transactions on Grap hics (SIGGRAPH) 25(3),2006,pp.527-532.

Peirce,J, Gray J.R, Simpson.S, MacAskill,M, Höchenberger R, Sogo,H, Kastman,E, Lindeløv,JK.2019.

RADIANT Ritsumeikan University Research Activities Bulletin, https://www.ritsumei.ac.jp/research/radiant/heart/story10.html/″(last accessed 24 Jan 2022).

R.L. Gregory: *Eye and Brain*. in M. Kondo, Y. Nakamizo and K. Miura (trans.), Brain and Vision - Gregory's Visual Psychology, Brain Publishing, (1998/2001).

Rodieck, R.W, "Quantitative analysis of cat retinal ganglion cell response to visual stimu li.", *Vision research*,5(11), 1965,pp.583-601.

Hiroyuki Sogo, Practical Python Library Psychology Experimental Programming - Experiment Creation and Data Processing with Python/PsychoPy, Asakura Shoten, 2017.

Tadashi Yamazaki, Hajimete no Neural Circuit Simulation - From One Neuron to a Human Omnipotent Model, Morikita Publishing, 2021.

.

9Chapter Acknowledgements.

I would like to express my sincere gratitude to Professor Michelette for her enthusiastic guidance during the course of this research. Without his sound advice and support, this research would not have been possible and could not have been compiled into this paper. Thank you very much.

I would also like to thank Mr Shunryo Yoshida of the laboratory for his kind and attentive guidance to me, as I had limited knowledge of programming and neural circuit simulation. He was always willing to answer my questions and gave me numerous advices. Also, when my research did not go well and I was stuck, Mr Yoshida's extensive knowledge of my research and his programming skills helped me many times. Thank you very much.

I had many discussions with my classmates and other members of the laboratory through weekly seminar activities. This stimulated me and I was able to make meaningful progress in my research through friendly competition with everyone. Thank you very much.

Last but not least, we would like to thank all the subjects who found time in their busy schedules to conduct the experiments in this study and who willingly agreed to participate in the experiments. Without your participation in the experiment, we would not have been able to carry out this study. Thank you very much.